Journal of Geophysical Research: Oceans

RESEARCH ARTICLE
10.1029/2018JC013939

A Numerical Study of Tropical Cyclone-Induced Sediment Dynamics on the Australian North West Shelf

François Dufois[1,2,3,4], Ryan J. Lowe[1,2,3], Matthew D. Rayson[1,3], and Paul M. Branson[1,3,5]

[1]The UWA Oceans Institute, University of Western Australia, Crawley, Western Australia, Australia, [2]ARC Centre of Excellence for Coral Reef Studies, University of Western Australia, Crawley, Western Australia, Australia, [3]Oceans Graduate School, University of Western Australia, Crawley, Western Australia, Australia, [4]IFREMER, DYNECO/DHYSED, Plouzané, France, [5]CSIRO Oceans and Atmosphere, Crawley, Western Australia, Australia

Abstract Owing to their strong forcing of the ocean surface, tropical cyclones strongly modify the hydrodynamics of Australia's North West Shelf (one of the world's tropical cyclone hot spots), which in turn plays a dominant role in its sediment dynamics. Previous modeling studies have focused on describing the short-term sediment dynamics during individual tropical cyclones but have lacked validation of the responses using field observations. As a consequence, the long-term cumulative impact of the tropical cyclones on the residual sediment transport pathways at the shelf scale remains unclear. In this study we apply a sediment transport model over the North West Shelf, validate its performance using an extensive field data set, and implement a 14-year-long model simulation to assess the sediment fluxes. The model results confirm the overwhelming role tropical cyclones play on sediment transport processes over most of the shelf, despite each cyclone only influencing a small portion of the shelf at a particular time. Overall, we identified 19 tropical cyclone events over the 14-year period, which, despite accounting for less than 5% of time, were found to drive the majority of both the suspended sediment alongshore and seaward cross-shore transport. The results revealed significant interannual variability of the tropical cyclone-induced sediment dynamics with greater suspended transport during the three consecutive Ningaloo Niño years (2011–2013) where sea surface temperatures off northwestern Australia were anomalously warm with elevated tropical cyclone activity.

Key Points:
- The Australia's North West Shelf ROMS-COAWST model reproduced the suspended sediment dynamics observed during historical tropical cyclones
- Over a 14-year period tropical cyclones dominate the overall sediment dynamics of the entire shelf despite being relatively infrequent
- Interannual variability of the sediment dynamics is simulated with increased cyclone activity during three consecutive warm Ningaloo Nino years

Supporting Information:
- Supporting Information S1

Correspondence to:
F. Dufois,
francois.dufois@uwa.edu.au

Citation:
Dufois, F., Lowe, R. J., Rayson, M. D., & Branson, P. M. (2018). A numerical study of tropical cyclone-induced sediment dynamics on the Australian North West Shelf. *Journal of Geophysical Research: Oceans*, *123*, 5113–5133. https://doi.org/10.1029/2018JC013939

Received 26 FEB 2018
Accepted 26 JUN 2018
Accepted article online 11 JUL 2018
Corrected 17 AUG 2018
Published online 3 AUG 2018

This article was corrected on 17 AUG 2018. See the end of the full text for details.

1. Introduction

Tropical cyclones (TCs), also described as hurricanes or typhoons depending on global origin, cause major damage to coastal infrastructures and ecosystems through their extreme wind and wave forcing (Larcombe & Carter, 2004; Liu et al., 2012; Madsen et al., 2001; Sherman et al., 2016; Tian et al., 2009; Wolanski et al., 2008). TCs have the capacity to drastically modify coastal and shelf sediment dynamics and in turn can destroy marine habitats (Tian et al., 2009), shape continental shelves (Larcombe & Carter, 2004), and drastically transform coastlines (Day et al., 2007; Lindemer et al., 2010; Stone et al., 2004; Wang et al., 2006). With an average of ~3 TCs per year, Australia's North West Shelf (NWS) is a TC hot spot in the Indo-Pacific region (Condie et al., 2009). In this economically important marine region, where oil, gas, and mineral export facilities coexist with high value marine ecosystems (Longley et al., 2002), TCs are known to strongly modify the shelf hydrodynamics (Drost et al., 2017; Hearn & Holloway, 1990; Rayson et al., 2015). As a consequence, TCs have been observed to play an important role in modulating the sediment dynamics over the shelf (Dufois et al., 2017) and drive major and rapid morphological changes along the coastline (Cuttler et al., 2018).

Although the influence of TC on the NWS has been an area of active research over many decades, Larcombe and Morrison-Saunders (2017) recently highlighted a number of major knowledge gaps, in particular, the need to identify the primary shelf-scale sediment transport pathways and geomorphological changes induced by extreme events over the region, which are also relevant to understanding TC prone continental shelf regions worldwide more generally. These long-term, shelf-scale sediment pathways can play a crucial role on coastal morphodynamics, shape benthic habitat distributions, and impact subsea industry activities. In general, for TC regions worldwide, in situ observations of the spatial variability of sediment dynamics in response to extreme TCs at the regional scale remain challenging to capture. Therefore, numerical modeling studies have been carried out in recent years to provide deeper insight (Beudin et al., 2017; Miles et al., 2015; Palinkas et al., 2014; Warner et al., 2010; Xu et al., 2016). Nevertheless, these modeling efforts have primarily focused on the short-term response of marine systems to specific TCs and not thus the integrated effect of a number of TCs on the cumulative shelf sediment dynamics. Similarly, over the NWS, previous modeling

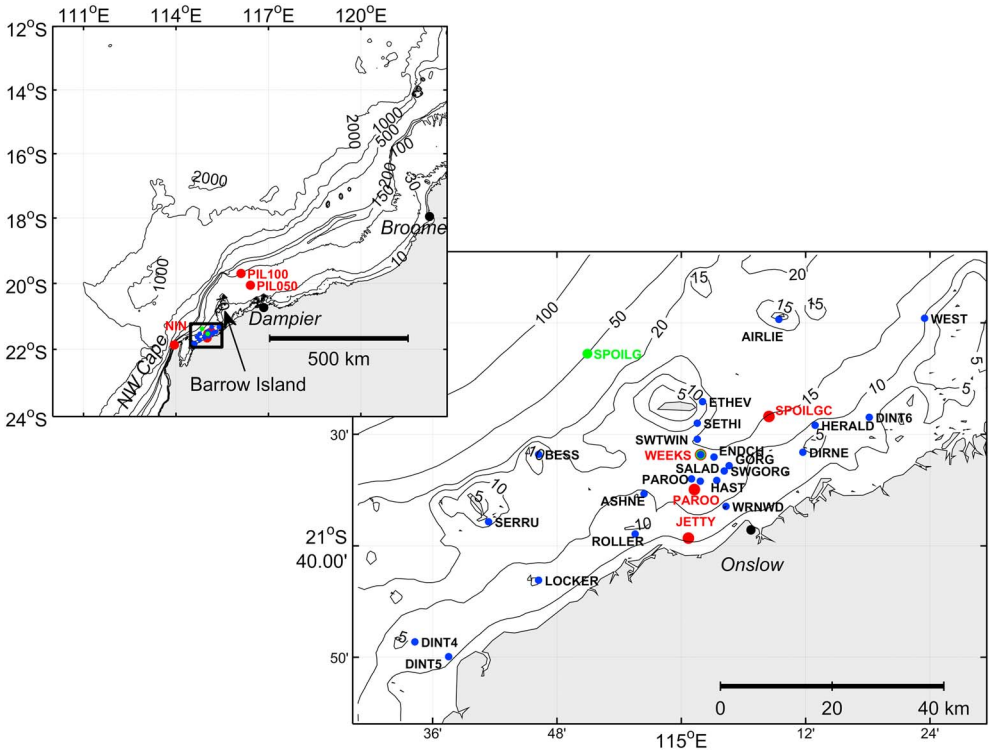

Figure 1. Study site, bathymetry and location of the various field instruments. Blue dots denote turbidity sensors, red dots represent current meters, and the green dots denote the wave buoy locations. The extent of the upper left panel corresponds to the model grid domain.

studies have (1) only considered the influence of one or two cyclones at a time (Condie et al., 2009; Margvelashvili et al., 2006) and (2) lacked in situ data to validate or support the results, thereby making it difficult to draw general conclusions about the role TCs play on the shelf sediment dynamics.

In this study we take advantage of an extensive 2-year-long in situ data set presented in a companion paper recently published (Dufois et al., 2017) as the foundation for the development of a process-based hydrodynamic-sediment transport model of Australia's northwest region. We then use the model to investigate the role of recurrent episodic TCs on the suspended sediment dynamics over plurennial timescales. We demonstrate that over the course of 14 years, episodic TCs dominate both the alongshore sediment transport over most of the shelf and sediment export off the shelf, despite these TCs occurring infrequently and the strong background forcing (largely tidally drive) that occurs in the region.

2. Methods

2.1. Numerical Model

The model was developed using the Coupled Ocean-Atmosphere-Wave-Sediment transport (COAWST) modeling system (Warner et al., 2010), in which the hydrodynamic Regional Ocean Modeling System (ROMS) model (Shchepetkin & McWilliams, 2005), the Simulating WAves Nearshore (SWAN) wave model (Booij et al., 1999), and the Community Sediment-Transport Modeling System sediment model (Warner et al., 2008) were coupled. For the present application of the COAWST system, the SWAN wave model was run independently and provided wave forcing for the sediment transport model.

The model was run on a 4-km horizontal resolution grid (321 × 318 cells) with 40 vertical sigma levels with increasing resolution near the surface and the bottom. The model included the NWS region between the North West Cape and Broome (note that the domain of the upper left panel in Figure 1 corresponds with the limits of the model grid). The bathymetry was extracted from the digital elevation model made available through the Western Australian Marine Science Institution Dredging Science Node (Sun & Branson, 2018), integrating the ~250-m resolution Geoscience Australia bathymetry (https://doi.org/

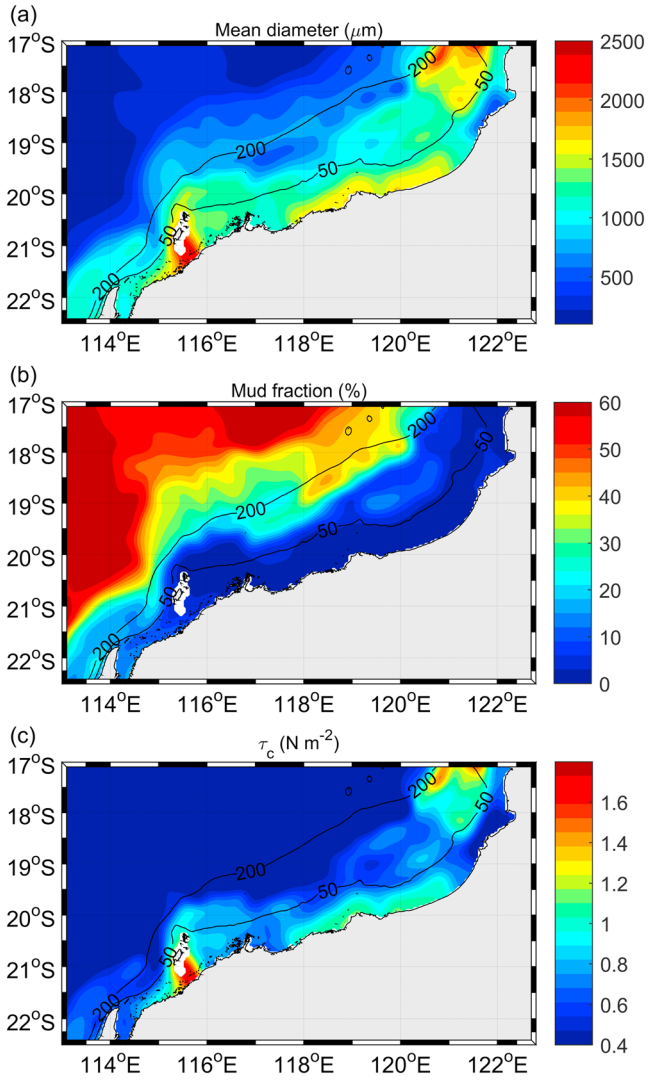

Figure 2. Model initial condition for (a) the mean sediment diameter, (b) the mud fraction, and (c) the critical shear stress. The 50- and 200-m isobaths are indicated for reference.

10.4225/25/53D99B6581B9A) and several industry bathymetric data sets. Hourly atmospheric forcing, including wind and air-sea fluxes, were obtained from the Climate Forecast System (CFS) reanalysis (Saha et al., 2010) and the CFS operational analysis (from April 2011 onward; Saha et al., 2014) at ~38-km horizontal resolution, which were used to force both the ROMS and SWAN models. The CFS reanalysis has been shown to satisfactorily reproduce TC events (Hodges et al., 2017).

2.1.1. Hydrodynamic Model

The ROMS model was initialized and forced at the open boundaries using the 1/12° global Hybrid Coordinate Ocean Model analysis (Chassignet et al., 2007). Tides were specified at the open boundaries using a Chapman condition (Chapman, 1985) forced by the Oregon State University global tidal solutions (TPXO7.1; Egbert & Erofeeva, 2002). This study used the k-ω parametrization of the generic length scale turbulence closure scheme (Warner et al., 2005). Horizontal eddy diffusivity and viscosity were fixed and both equal to 5 m^2/s. A similar ROMS configuration has previously been applied successfully to the NWS to study the hydrodynamic response to TCs (Rayson et al., 2015).

2.1.2. Wave Model

In our study the SWAN wave model accounted for both wind-wave generation within the model domain and wave transmission coming in from the boundaries. The model was forced at the boundaries using wave height (H_s) and peak period (T_p) from The Centre for Australian Weather and Climate Research wave hindcast at 4′ (~7 km) resolution based on the Wavewatch III model (Durrant et al., 2014; Hemer et al., 2016; http://doi.org/10.4225/08/523168703DCC5). The frequency domain was discretized on a logarithmic scale into 37 frequency bins, ranging from 0.03 to 1 Hz. The directional domain was discretized into 36 bins of 10°. We used the whitecapping source term derived from van der Westhuysen et al. (2007), combined with the wind input term provided by the Yan (1987) formulation. Depth-limited wave breaking was calculated based on the Battjes and Janssen (1978) formulation using a default breaking index value of $\gamma = 0.73$. The bottom friction was computed using the Madsen et al. (1988) formulation with a roughness length scale of 0.05 m. The SWAN model has previously been applied to the NWS and showed good agreement with in situ data in the vicinity of TCs (Drost et al., 2017).

2.1.3. Sediment Model

We initially performed extensive model tests that were compared with in situ and calibrated satellite remote sensing data detailed in Dufois et al. (2017; see section 2.2 below) to select an optimal set of plausible and efficient parameters for the sediment model. No model sensitivity analyses is presented in this study, and validation of only the best model run is described in detail with model performance statistics.

We used the SSW_BBL bottom boundary layer scheme defined by Warner et al. (2008), which implements the model of Madsen (1994) to compute the sum of the wave- and current-induced stress. The bed roughness was only composed of the grain roughness (spatially varying as a function of the modeled median diameter). Including the bedform roughness and the sediment transport roughness (i.e., the roughness induced by moving sediment) was only found to decrease the overall model performance.

The bed sediment distribution was initialized using grain size properties obtained through the Marine Sediment database from Geoscience Australia (http://www.ga.gov.au/metadata-gateway/metadata/record/69869/). Seven sediment classes were considered in the model, including one class of mud (composed of silt and clay with mean diameter of 32 μm), five classes of sands (100, 190, 375, 750, and 1,500 μm), and one class of gravel (5,000 μm). Considering only one class of mud was related to the hypothesis that the settling velocity for muds is controlled by flocculation processes, and that individual grain sizes do not directly impact

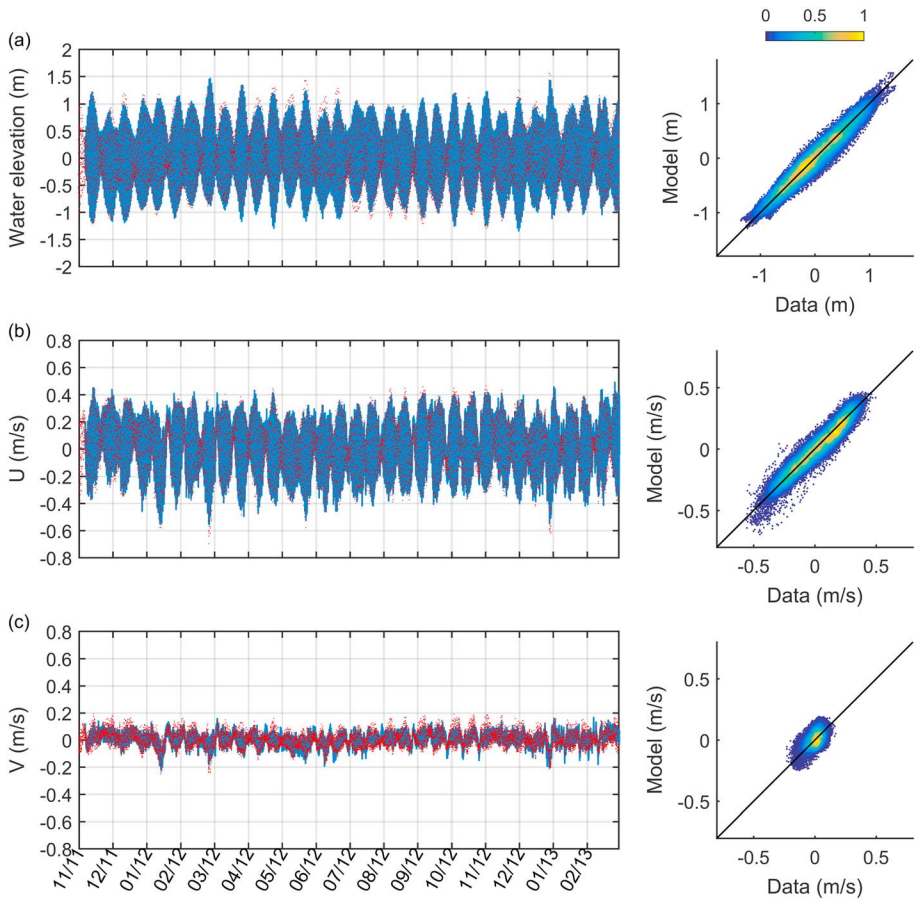

Figure 3. Comparison between hourly in situ data (in blue) and model results (in red) at PAROO for (a) water elevation anomalies and depth averaged eastward (b) and northward (c) velocity components. Left panels are time series. Right panels are scatter plots of model values against in situ values (color bar indicates the point density). Comparisons at other locations are given in supporting information Figures S1–S3.

settling processes. Due to the overwhelming impact of sediment resuspension compared to sediment river discharge (Dufois et al., 2017), no sediment inputs by rivers were considered in this study. The sediment bed was initially composed of nine layers of 5-cm thickness plus a bottom layer of 5 m, before freely evolving due to successive erosion and deposition processes.

The main focus of our study is on the suspended sediment dynamics because no data were available to calibrate and validate bedload transport. Although bedload was included in the model, we only discuss it briefly below in the context of its potential implications. The gravel and sand classes were only transported through bedload using the formulation of Soulsby and Damgaard (2005). The mud class was transported by suspended load only, and the mass of sediment available for suspended transport was limited to the mass of sediment available in an active layer computed using the formulation of Wiberg and Harris (1994). Sensitivity tests were performed to optimize the choice of different parameters necessary for the suspended sediment transport model. The formulation of Ariathurai and Arulanandan (1978) for the erosion flux has been modified to test the effect of the power to which the excess shear stress is raised, and in the end we chose a power of 1.5 that is usually used for sands (van Rijn, 1984). The bed erodibility constant was calibrated and chosen to be 5×10^{-5} kg·m^{-2}·s^{-1}. The settling velocity was set to 0.1 mm/s, which is consistent with the range of values encountered for small mud flocs (Soulsby et al., 2013; Verney et al., 2009).

We modified the Community Sediment-Transport Modeling System sediment model to compute the critical shear stress for both suspended load and bedload as a function of the sediment diameter (Wilcock, 1993). The sediments of the NWS are relatively coarse but poorly sorted and composed of a wide spread range of sediment sizes from mud to gravel (Figure 2). For sediment mixtures, numerous formulations (often

diverging) have been proposed in the literature to estimate the critical shear stress of each sediment classes, but no universal relationship is accepted (Buffington & Montgomery, 1997; van Rijn, 2007). Wilcock (1993) suggested that using the critical shear stress of the sediment mixture mean diameter τ_{cm} computed using Shield's formulation for all sediment classes was a good first approximation for unimodal or slightly bimodal sediment distribution. Similarly, van Rijn (2007) showed that using the same critical shear stress (computed from the median diameter Shields parameter) for all sediment classes was a good compromise for a wide range of sediment mixture. We tested these two formulations, together with two others (Egiazaroff, 1965; Wu et al., 2000) and, after comparison with the field observations, adopted the Wilcock (1993) formulation for subsequent simulations. Hence, in the model outputs provided in this study, all sediment classes, including muds, had the same critical shear stress τ_{cm}. The spatially variable critical shear stress initially ranged ~0.5–1.5 N/m^2 over the shelf (Figure 2c) and was allowed to evolve throughout the simulation as the bed composition changed.

When considering the entire shelf, the region around Barrow Island clearly stood out due to large overestimations in our initial model runs when comparing the model outputs of suspended sediment concentration (SSC) with remote sensed data. The source of sediment initially present in this shallow region, composed of large and dense fields of macroalgae, appeared unrealistic. Therefore, we used benthic habitat maps available through the Pilbara Marine Conservation Partnership (https://research.csiro.au/pmcp/) to precondition the sediment bed cover within the region in the vicinity of Barrow Island. No initial sediment was considered to be present in these areas, while sediment resuspension and bedload processes were switched off in this macroalgae-dominated region around Barrow Island (white region in Figure 2).

2.1.4. Model Scenarios

The model run spanned January 2002 to December 2015, corresponding to a period studied in detail using field observations described in our companion paper (Dufois et al., 2017), when calibrated Moderate Resolution Imaging Spectroradiometer (MODIS) Aqua- and Terra-derived SSCs were also available (see section 2.2.1) for validation. In order to perform this ~14-year-long model run, only the one-way coupling (SWAN to ROMS) was activated to improve computational efficiency. The SWAN model was run first and provided wave forcing parameters to the ROMS hydrodynamic/sediment transport model. Note that the model at this resolution does not resolve a potential surf zone region near the coastline and hence potential wave-driven alongshore currents (littoral drift) and thus would not capture the alongshore sediment fluxes at the coastline that would be responsible for processes such as coastal erosion. At locations where moorings were present, model results were output hourly to allow for direct comparisons. Over the entire model domain, only daily averaged values were saved for analysis to limit excessive data output.

2.1.5. Model-Derived Variables

We estimated the contribution of advection/diffusion and net erosion/deposition sediment fluxes to the local rates of change of sediment concentration by depth-integrating the three-dimensional advection-diffusion equation as

$$\underbrace{\int_{-h}^{\eta}\frac{\partial c}{\partial t}\mathrm{d}z}_{(1)\text{ Rate of change}} = \underbrace{-\int_{-h}^{\eta}\left(\frac{\partial uc}{\partial x}+\frac{\partial vc}{\partial y}\right)\mathrm{d}z+\int_{-h}^{\eta}\left(\frac{\partial}{\partial x}\left(K_H\frac{\partial c}{\partial x}\right)+\frac{\partial}{\partial y}\left(K_H\frac{\partial c}{\partial y}\right)\right)\mathrm{d}z}_{(2)\text{ Horizontal advection and diffusion}}+\underbrace{E-D}_{(3)\text{ Net erosion/deposition sediment flux}} \quad (1)$$

where c is the sediment concentration, h is the bottom depth, η is the free surface elevation, u and v are the horizontal velocity components, K_H is the horizontal turbulent diffusivity, E is the erosion flux, and D is the deposition flux. Note that all flux terms were computed directly in the model and saved as daily averaged diagnostic terms for this analysis. We then computed the *vertical flux contribution* R_h as

$$R_h = \frac{E-D}{\left|-\int_{-h}^{\eta}\left(\frac{\partial uc}{\partial x}+\frac{\partial vc}{\partial y}\right)\mathrm{d}z+\int_{-h}^{\eta}\left(\frac{\partial}{\partial x}\left(K_H\frac{\partial c}{\partial x}\right)+\frac{\partial}{\partial y}\left(K_H\frac{\partial c}{\partial y}\right)\right)\mathrm{d}z\right|} \quad (2)$$

This parameter provides insight into the relative importance of local vertical fluxes to/from the bed to the horizontal fluxes while preserving the sign of the net vertical fluxes (i.e., if R_h is positive erosion overcome deposition and vice versa).

To evaluate the contribution of TC events to the total cumulative sediment flux (for both suspended load and bedload) over the 14-year study period, we computed the *TC contribution* R_{TC} at each grid cell as follows:

Table 1
Correlation Coefficient (R), Bias (BIAS), Root-Mean-Square Error (RMSE), Scatter Index (SI), and Willmott Index (WIL) at Six Different Sites for the Water Elevation, the Hourly U and V Depth-Averaged Velocity Components, and the Daily Averaged Alongshore and Cross-Shore Depth-Averaged Velocity Components

	R	*SI* (%)	*RMSE*	*BIAS*	*WIL*
Site			Water elevation (m)		
PAROO	0.97	24.2	0.12	0.0048	0.98
SPOILGC	0.97	24.2	0.13	−0.0026	0.99
WEEKS	N/A	N/A	N/A	N/A	N/A
JETTY	0.97	26.3	0.13	−0.0058	0.98
NIN	0.92	40.5	0.14	0.0011	0.96
PIL100	0.89	45.2	0.34	0.0078	0.94
PIL050	0.99	16.1	0.13	0.0096	0.99
			U (m/s)		
PAROO	0.96	27.9	0.052	−0.0076	0.98
SPOILGC	0.97	25.1	0.054	0.004	0.98
WEEKS	0.94	39.9	0.10	−0.015	0.95
JETTY	0.93	40.1	0.067	0.01	0.96
NIN	0.61	83.6	0.14	−0.012	0.78
PIL100	0.63	77.0	0.19	−0.0024	0.76
PIL050	0.76	68.1	0.18	−0.052	0.84
			V (m/s)		
PAROO	0.51	112	0.051	0.0021	0.71
SPOILGC	0.73	68.1	0.042	−0.0015	0.83
WEEKS	0.60	80.1	0.069	−0.015	0.70
JETTY	0.29	189	0.067	0.025	0.47
NIN	0.63	82.7	0.16	−0.047	0.77
PIL100	0.61	84.4	0.16	−0.058	0.71
PIL050	0.70	76.3	0.15	−0.068	0.77
			Daily averaged alongshore current (m/s)		
PAROO	0.86	52.4	0.043	0.0062	0.92
SPOILGC	0.86	51.4	0.042	0.0023	0.92
WEEKS	0.80	64.2	0.078	−0.021	0.82
JETTY	0.83	59.4	0.046	0.00069	0.91
NIN	0.70	78.0	0.17	−0.056	0.82
PIL100	0.48	88.9	0.18	−0.032	0.59
PIL050	0.78	78.1	0.16	−0.076	0.72
			Daily averaged cross-shore current (m/s)		
PAROO	−0.042	112	0.014	0.0051	0.33
SPOILGC	0.0013	124	0.017	−0.0036	0.37
WEEKS	−0.023	103	0.025	−0.0046	0.26
JETTY	0.20	416	0.056	0.026	0.20
NIN	0.14	105	0.0060	−0.020	0.40
PIL100	0.32	97.5	0.11	−0.049	0.49
PIL050	0.18	96.1	0.087	−0.040	0.43

Note. N/A = not available.

$$R_{TC} = \frac{\sum_j \left| \overrightarrow{\phi_j} \right|}{\sum_i \left| \overrightarrow{\phi_i} \right|} \quad (3)$$

where $\overrightarrow{\phi}$ is the daily integrated sediment flux directly computed and saved in the model. The *i* index denotes all days included during the 14-year simulation, while the *j* index only indicates the days when cyclones were present within the model domain and a week after they exit the domain or dissipate.

We also computed the cumulative suspended sediment flux vector $\overrightarrow{\Phi_c}(t)$:

$$\overrightarrow{\Phi_c} = \int_{t1}^{t} \overrightarrow{u(t)} c(t) \mathrm{d}t \quad (4)$$

where $\overrightarrow{u(t)}$ and $c(t)$ are the velocity vector and the sediment concentration at time t, and t_1 is the initial time for the integration. At stations (where moorings were present) the integration was performed using hourly output, while over the entire domain the integration was performed using the daily integrated sediment flux $\overrightarrow{\phi}$ computed in the model.

2.2. Model Evaluation

2.2.1. Data Used for Model Evaluation

The field observations used in this study to evaluate the model performance were previously described in detail in Dufois et al. (2017), so only a brief summary is included below. It includes in situ observations from different sources for various locations across the Pilbara region of the NWS, including wave buoys, acoustic current meters/profilers, turbidity sensors, and sediment traps for the period spanning May 2011 to March 2013. We used data from three acoustic current profilers from the Integrated Marine Observing System available at https://portal.aodn.org.au/ (sites NIN, PIL050, and PIL100 in Figure 1). All of the other in situ data were acquired as part of the Wheatstone project environmental management framework (Chevron, 2011, 2016) and made available through the Western Australian Marine Science Institution Joint Venture. This data set comprised a set of bottom-mounted sensors deployed over a section of the shelf centered off Onslow, including 23 turbidity sensors, 20 sediment traps, 2 wave buoys, 3 current profilers, and 1 current meter (Figure 1, for more details see Table 1 of Dufois et al. (2017)).

The turbidity sensors that were deployed were not individually calibrated to SSC with in situ sediment. For model comparison purpose we therefore assumed a direct relationship between turbidity and SSC (i.e., 1:1 slope and no intercept), which is consistent with an in situ calibration performed posteriorly in the area with a similar turbidity sensor (slope of 1.07; Dufois et al., 2017; Sun & Branson, 2018). Note that the near-bottom SSC estimated from the turbidity sensors could, however, be over or underestimated since the turbidity to concentration slope can vary below or above 1 (Rügner et al., 2013). The slope generally increases when the particle size increases (Bunt et al., 1999), and therefore, an underestimation of the SSC could happen during TC events since suspended sediment particles tend to be coarser (Dufois et al., 2017).

We also used the MODIS Aqua- and Terra-derived SSC products at 250-m resolution for the period between June 2002 and December 2015, as processed by Dorji et al. (2016) using a semianalytical model calibrated and validated specifically for the coastal waters within the same Pilbara study region (available at http://remote-sensing.nci.org.au/). We constructed a composite of the two products at the weekly timescale at 4-km resolution in order to have fewer gaps in the data set for subsequent analysis.

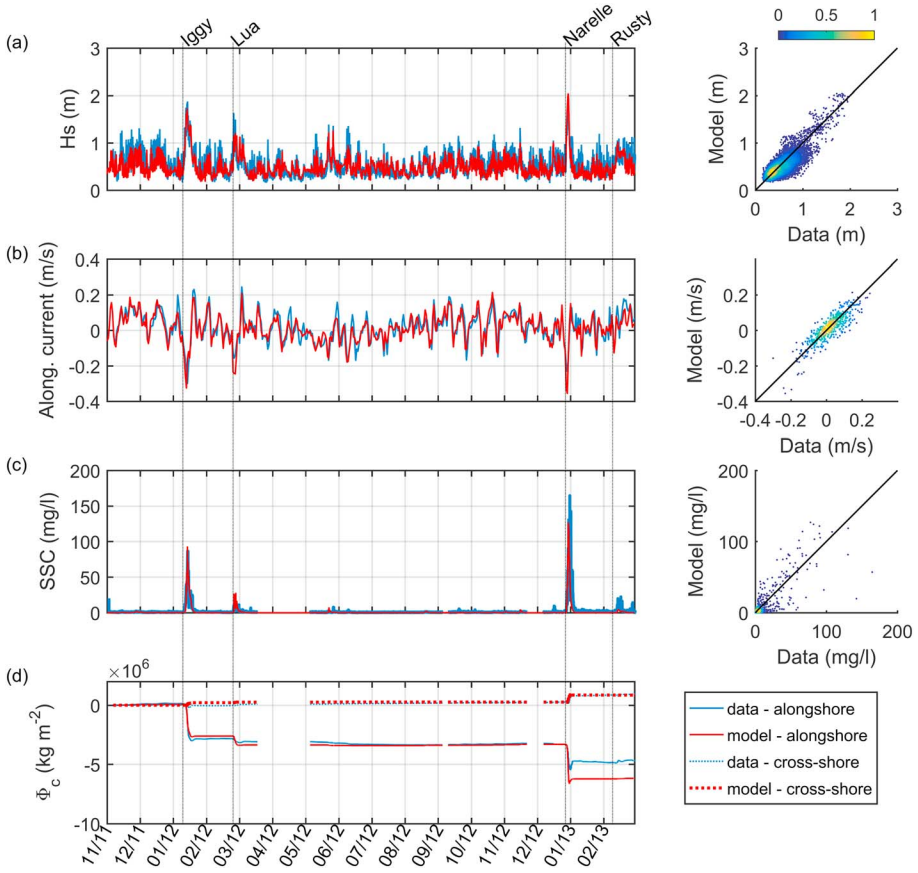

Figure 4. Comparison between hourly in situ data (in blue) and model results (in red) at PAROO for (a) significant wave height, (b) depth-averaged alongshore current velocity, (c) bottom sediment concentration, and (c) cumulative alongshore and cross-shore bottom sediment fluxes. Right panels are scatter plots of model values against in situ values (color bar indicates the point density). The alongshore axis is positive in the northeastward direction, and the cross-shore axis is positive seaward. Comparisons at other locations are given in supporting information Figures S4 and S6–S8.

2.2.2. Model Performance Metrics

The model performance was evaluated using the correlation coefficient (R), the bias (BIAS), the root-mean-square error (RMSE), the scatter index (SI), and the Willmott index (WIL; Willmott, 1982):

$$R = \frac{\sum_{i=1}^{N} (O_i - \overline{O})(P_i - \overline{P})}{\sqrt{\sum_{i=1}^{N} (O_i - \overline{O})^2 \sum_{i=1}^{N} (P_i - \overline{P})^2}} \tag{5}$$

$$BIAS = \overline{P} - \overline{O} \tag{6}$$

$$RMSE = \sqrt{\frac{\sum_{i=1}^{N} (O_i - P_i)^2}{N}} \tag{7}$$

$$SI = \sqrt{\frac{\sum_{i=1}^{N} (O_i - P_i)^2}{\sum_{i=1}^{N} O_i^2}} \tag{8}$$

Table 2
Model Performance Metrics at Five Different Sites for the Significant Wave Height

Site	*R*	*SI* (%)	*RMSE* (m)	*BIAS* (m)	*WIL*
SPOILG	0.92	19.9	0.21	−0.0020	0.95
WEEKS	0.79	27.6	0.17	0.035	0.88
SPOILGC	0.83	28.1	0.17	0.079	0.89
PAROO	0.81	24.3	0.14	−0.037	0.89
JETTY	0.80	49.6	0.23	−0.18	0.61

Note. R = correlation coefficient; SI = scatter index; RMSE = root-mean-square error; BIAS = bias; WIL = Willmott index.

$$WIL = 1 - \frac{\sum_{i=1}^{N} (P_i - O_i)^2}{\sum_{i=1}^{N} \left(\left|P_i - \overline{O}\right| + \left|O_i - \overline{O}\right|\right)^2} \quad (9)$$

where O_i is the observed value at time step i, P_i the predicted value at the same time step, and $\overline{O}$ and $\overline{P}$ are, respectively, the mean values of O_i and P_i for the N time steps.

The *SI* corresponds to the relative RMSE where the denominator in equation (8) represents the root-mean-square of the observed values. Lower *SI* values correspond to better agreement between the model and the observations. For example, a *SI* value of 100% means that the RMSE is as big as the root-mean-square value. *WIL* is bounded by 0 and 1, with a value of 0 corresponding to complete disagreement between the model and the observation and 1 corresponding to a complete agreement.

We mostly based the model validation discussion around the Willmott skill score in the following sections. Other model performance metrics are listed for completeness and also to aid in further diagnosis of areas of poorer model performance.

3. Model Validation

3.1. Hydrodynamics

The hourly water elevations predicted by the model, which were strongly tidally driven, were in good agreement with the field observations at the six locations over the shelf (Figures 3a and S1 in the supporting information), with good overall model performance metrics (Table 1), including *WIL* ranging 0.94–0.99. The model performance tended to be slightly poorer at the two deepest sites NIN and PIL100 (Table 1).

Similarly, the depth-averaged current velocities were well reproduced by the model (Figures 3b, 3c, S2, and S3 and Table 1). Over the shallower sites, PAROO, SPOILGC, WEEKS and JETTY, WIL for currents along the *x* axis (west-east) ranged from 0.95 to 0.98. Lower model skill occurred for currents directed along the *y* axis (south-north), with *WIL* ranging 0.47–0.83, as a consequence of the relatively small current amplitudes in that direction. For the west-east velocity component, the model performance slightly decreased for the three deepest sites, with *WIL* ranging 0.76–0.84, consistent with the lower correlation values.

We used the daily averaged model output to infer the depth-averaged subtidal current variability. Since subtidal currents are mostly in the alongshore direction off Onslow (Dufois et al., 2017), the subtidal currents were rotated according to the orientation of the local isobath (based on smoothing the isobath by applying a running mean with a 50-km-wide window) at each site and model grid cell. In good agreement with the observations, the modeled subtidal currents were mostly alongshore (Figures 4b, S4, and S5 and Table 1). The best model performance was achieved at the four shallowest sites, with *WIL* ranging from 0.82 to 0.92 in the alongshore direction. Model skill tended to decrease at the deeper sites, but performance was still deemed satisfactory at NIN and PIL050, where *WIL* ranged from 0.72 to 0.82. At the deepest site close to the shelf edge (PIL100), the model performance decreased, with *WIL* = 0.59 with lower correlation (R = 0.48).

The wave model performance was satisfactory across the shelf (Figures 4a and S6 and Table 2). As expected, the model performed best for the significant wave height at the deepest site (*WIL* = 0.95 at SPOILG, 52-m depth), where wave-seabed interactions (and hence shallow water wave transformations) are limited. At most other locations further inshore, the overall model performance remained satisfactory, with *WIL* ranging 0.88–0.89. The model performance, however, significantly decreased at the nearshore site JETTY (8-m depth), with *WIL* = 0.61, mostly because of some persistent model underestimation (*BIAS* = −0.18 m).

3.2. Sediment Dynamics and TC Events

Here we evaluated the model performance by comparing the modeled near-bottom SSCs with the in situ turbidity available near the bottom at each site. Although the turbidity sensors were not individually calibrated, the in situ turbidity is hereafter referred as SSC for consistency in reporting the model performance (which is reasonable considering the calibration curve obtained in the region posteriorly with a similar turbidity sensor). Overall, the model performed reasonably well at simulating the observed near-bottom SSCs at the 23 sites off Onslow (Figures 4c and S7 and Table 3). For 12 of the sites, the *WIL* was over 0.9, and 18 sites had *WIL* $>$ 0.8. However, some of the site-specific SSC variability was not well captured ($R < 0.7$ for the two sites: BESS and SWTWIN).

Table 3
Model Performance Metrics at 23 Different Sites Shown in Figure 1 for the Near-Bottom Suspended Sediment Concentrations

Site	*R*	*SI* (%)	*RMSE* (kg/m^3)	*BIAS* (kg/m^3)	*WIL*
AIRLIE	0.83	56.9	1.6	−0.62	0.89
ASHNE	0.90	74.1	3.7	−0.19	0.90
BESS	0.80	380	5.6	0.46	0.49
DIRNE	0.84	74.2	5.1	−0.69	0.88
ENDCH	0.93	39.8	2.1	−1.0	0.95
ETHEV	0.76	75.7	2.1	−0.42	0.85
DINT4	0.89	51.1	14	−2.6	0.94
GORG	0.86	51.0	4.0	−1.2	0.91
HAST	0.74	118	5.2	−0.34	0.78
HERALD	0.86	55.3	2.9	−0.77	0.92
LOCKER	0.90	72.4	7.3	−1.3	0.90
PAROO	0.92	42.8	1.6	−0.24	0.95
ROLLER	0.81	64.0	4.4	−1.2	0.88
SALAD	0.85	55.0	3.7	−0.80	0.92
SERRU	0.72	256	8.3	0.70	0.57
SETHI	0.78	65.1	1.6	−0.85	0.82
SWGORG	0.87	50.1	3.8	−1.2	0.92
SWTWIN	0.67	79.8	6.2	−1.7	0.60
WEEKS	0.89	45.3	3.7	−1.0	0.94
WEST	0.46	84.6	3.5	−0.47	0.54
WRNWD	0.82	65.9	5.3	−1.3	0.89
DINT6	0.84	53.8	5.9	−1.7	0.90
DINT5	0.85	51.9	17	−5.7	0.91

Note. *R* = correlation coefficient; SI = scatter index; RMSE = root-mean-square error; BIAS = bias; WIL = Willmott index.

Dufois et al. (2017) showed that the sediment dynamics during the 2-year field observation period (2011–2013) were dominated by TCs Iggy and Narelle. At two of the sites over the shelf (PAROO and WEEKS), there were colocated wave, current, and turbidity data available to estimate the model performance during TC events. Modeled and in situ wave heights and alongshore currents were in good agreement during Iggy and Narelle at those two sites, and both the SSCs and sediment fluxes were satisfactorily predicted (Figures 4 and S8). At PAROO, a slight overestimation of the alongshore southwestward current during Narelle led to some overestimation of the sediment fluxes during this event. At WEEKS, the underestimation of the alongshore southwestward current during Iggy and underestimation of the SSC during Narelle led to an underestimation of the total cumulative sediment flux. Overall, the patterns of SSC and both alongshore and cross-shore sediment fluxes in response to TCs were reproduced reasonably well.

In order to gain confidence in the longer-term model prediction, the modeled surface SSC were also compared to the MODIS SSC over the full 14-year-long period. There was generally satisfactory model agreement with the observations over the shallow shelf (<30 m) apart from some regions close to the coast and within the shadow of Barrow Island (Figure 5). Overall, 60% of the shelf area below 30-m depth had *WIL* greater than 0.4 (and $WIL > 0.3$ for 88% of the shelf below 30 m; Figure 5c). Areas with lower *WIL* index generally corresponded with areas with increased bias and/or decreased correlations (Figures 5a and 5b). The best model skill scores were found toward the southern part of the shelf where the in situ data originated. Considering only the period 2011–2013 for the comparison only led to a slight improvement of the model skill scores ($WIL > 0.4$ for 65% of the shelf below 30 m). Values of *WIL* based on the satellite observations were generally lower than the ones obtained using in situ data; however, some discrepancy between model performance metrics based on the surface satellite data with metrics based on bottom in situ turbidity data could be expected. First, the accurate prediction of surface SSC requires accurate prediction of both the sediment source terms at the bottom and the vertical SSC distribution. Second, there is additional uncertainty in the value of satellite-derived SSC compared with in situ measurements. Remote sensing algorithms have their own uncertainties; therefore, discrepancies between the model and the satellite-derived data cannot solely be attributed to the model. For instance, the apparent poor model skills in the deep ocean, where SSC values were relatively small, were primarily due to low signal-to-noise ratio in the satellite-derived SSC.

3.3. Model Sensitivity

Although not shown in this study, through inspection of the results it appeared that most of the sediment transport parameters (regarding the settling velocity, the erosion fluxes, and the critical shear stress) had little impact on the general patterns and variations in the sediment dynamics. However, the absolute magnitude of the response to a TC showed some level of dependence on the choice of the parameter values. For example, the SSC amplitude increased with the bed erodibility constant if all other parameters remained the same, although the SSC temporal variability was in good agreement with the data irrespective of the value of this parameter. We therefore acknowledge that the exact values of the sediment fluxes should be treated with some caution, especially in regions where no model validation with in situ observations could be performed.

We also note that the initial sediment cover had a major impact on the spatial variability of the sediment fluxes in some regions, mostly because erosion of fine sediments is a function of the proportion of each sediment class within the seabed. The sediment cover data are relatively scarce or even completely void of any sampling, in some areas of the shelf. Assigning a single representative sediment size distribution over a 4- by 4-km grid cell based on limited data points would enhance model parameter uncertainty. The initial sediment cover map might therefore not be fully representative of the true sediment distribution in certain areas. For example, the rather coarse sediment cover South of Barrow Island, inducing high critical shear stress values, may not be fully representative of the region, as it is based on only a few data points available in this area. It appeared that in this

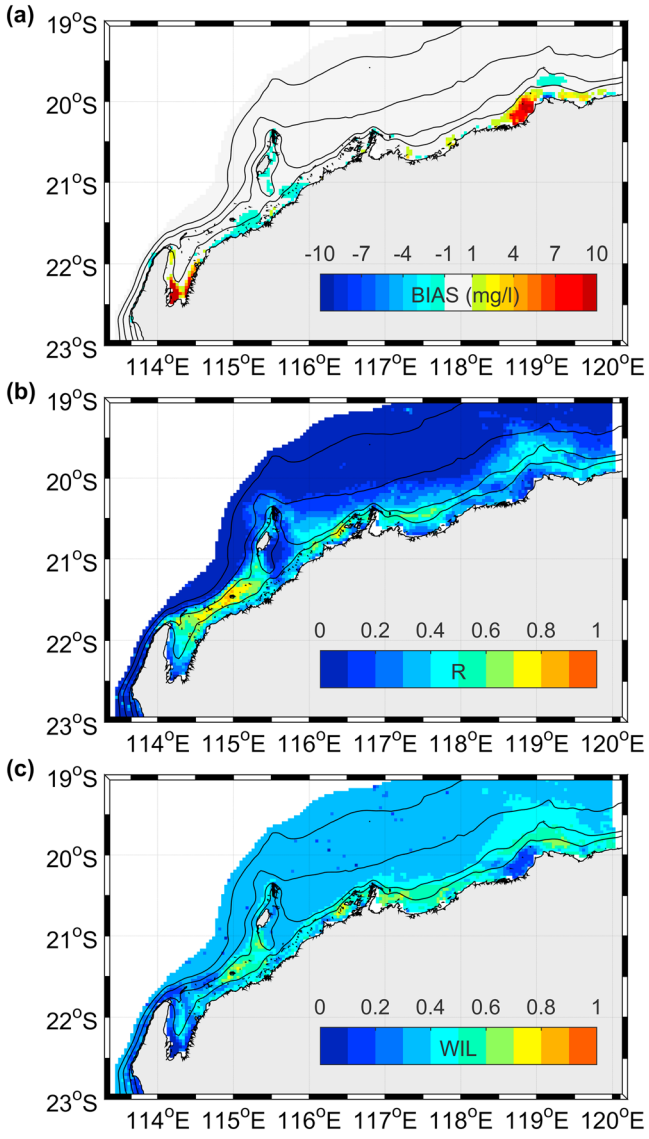

Figure 5. (a) Bias, (b) correlation coefficient, and (c) Willmott's skill between modeled surface SSC and MODIS SSC over the period of the MODIS SSC data (June 2002 to December 2015). The 10-, 20-, 50-, and 100-m isobaths are indicated for reference. Only depth shallower than 200 m are shown. SSC = suspended sediment concentration; MODIS = Moderate Resolution Imaging Spectroradiometer.

region the model performed most poorly when compared with the satellite-derived SSC estimates. We tried assuming various sediment cover in this region and found that it did not improve model performance; therefore, higher-resolution sediment cover data could be beneficial in such areas.

We also tested a fully coupled configuration (SWAN/ROMS with two-way coupling) during the ~2-year period when in situ data were available; however, the changes to the overall model skill were negligible. We are therefore confident that, at the resolution of the model configuration, using one-way coupling between SWAN and ROMS in order to improve computational efficiency for the ~14-year-long model run had little impact on the results that we present in this study.

4. Results

4.1.1. Model Results: Detailed 2011–2013 Period

Offshore Onslow, most of the sediment resuspension and transport over the shelf occurred during TCs Iggy and Narelle, with a global alongshore southwestward sediment transport simulated by the model over the shelf (Figures 4 and S8). However, outside of the region where field observations were available (i.e., at the scale of the entire shelf), those two TCs were not the only drivers of the sediment dynamics according to the model. Some other remote TCs along the northern section of the NWS also had an influence on the shelf. Indeed, in terms of wind and wave forcing, while Iggy and Narelle dominated over the southern part of the shelf along the 20-m isobath, Lua and Rusty induced the strongest winds and highest wave heights over the northern part of the shelf (Figures 6b and 6c; note that detailed zoomed results around the TCs are included in supporting information Figure S9). The wind and the subtidal currents appeared to be well correlated (Figures 6b and 6d), with R ranging from 0.75 to 0.9 between the alongshore current velocity and the alongshore wind speed along the 20-m isobath, except in the region near (~100 km) Barrow Island. During the four above mentioned TCs, the peak SSCs coincided with the period of peak wave heights across the shelf, and the onset of the wave/turbidity events was globally synchronous with southwestward winds and currents (Figures 6–8). During Iggy and Narelle, although the highest SSCs were predicted over the southern part of the shelf, elevated SSCs were predicted across the entire shallow portion of the shelf $<$30 m (Figure 7). By decomposing the total erosion flux into its wave and current contributions, we find that over most of the shelf the dominant driver of net sediment fluxes at the seabed was due to wave-induced resuspension, except within a narrow coastal strip (10 to 20 km from shore) where current-induced resuspension dominated (Figures 9a and 9b). Subtidal southwestward currents were only predicted to occur toward the southern part of the shelf; as a consequence, residual southwestward alongshore sediment fluxes were significant only over that part of the shelf (Figure 6f). During Lua and Rusty, sediment resuspension occurred mostly in the northern region of the domain where there were also strong southwestward subtidal flows (Figures 8 and 9), together acting to drive strong southwestward sediment fluxes (Figure 6f). In this same region there was a reversal of the currents to the northeast after the passage of both TCs (Figure 6d), leading to northeastward alongshore sediment fluxes (although smaller than the earlier southwestward flux; Figures 4d, S8d, and 6f). Waves were clearly the main forcing mechanism of sediment resuspension, except close to the coast and offshore of the 50-m isobath during Rusty, where currents made a dominant contribution to the sediment resuspension (Figures 9a and 9b).

During the peak (i.e., the increasing phase of the SSC signal) of all four TC events (Iggy, Lua, Narelle, and Rusty), the net erosion/deposition fluxes were generally larger than the horizontal advective and diffusive fluxes over most of the shelf at the daily timescale (Figures 6g, 6h, 9c, and supporting information

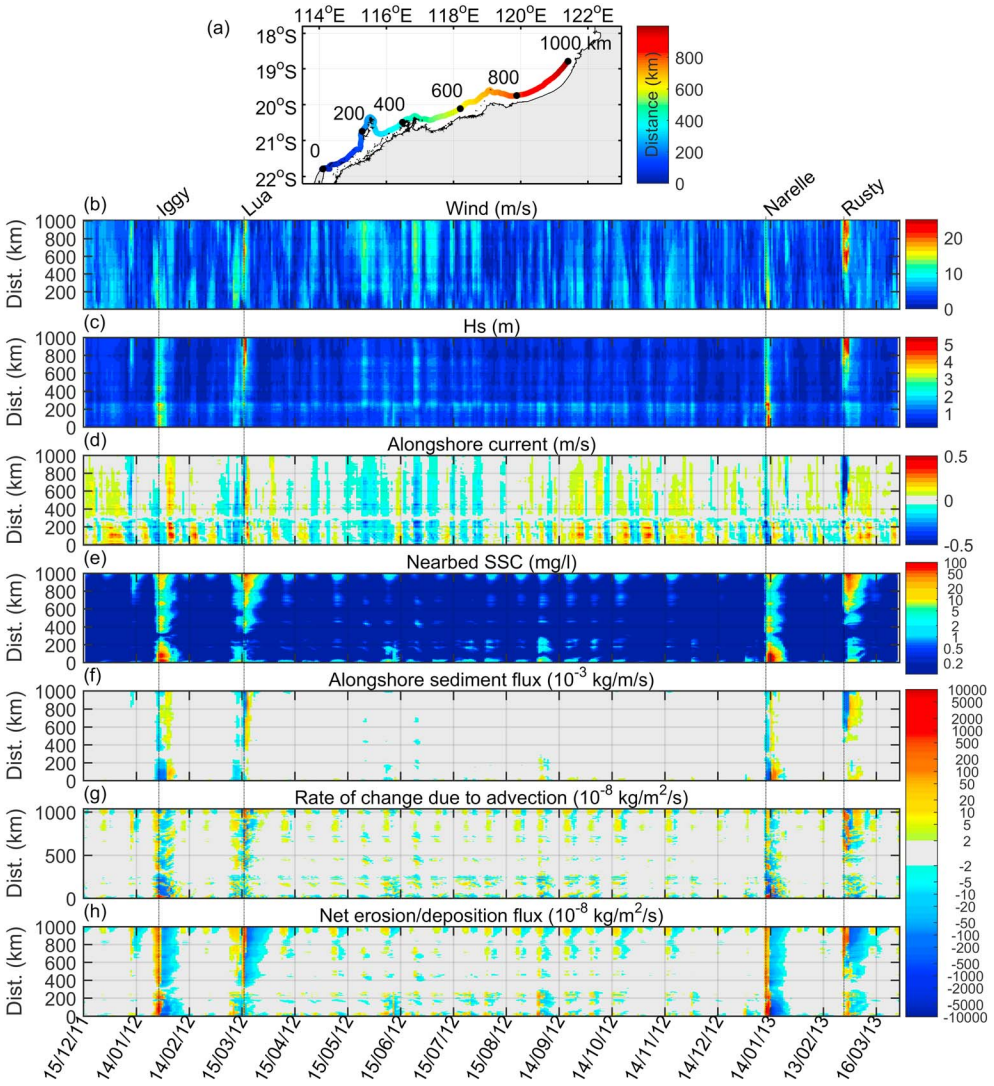

Figure 6. Sediment dynamics simulated by the model along the 20-m isobath shown on panel (a) for the period spanning December 2011 to March 2013. (b) Wind strength, (c) significant wave height, (d) alongshore current velocity, (e) bottom sediment concentration, and (f) depth-integrated alongshore sediment flux. Depth-integrated sediment concentration rate of change due to (g) advection and diffusion and (h) net erosion/deposition flux. For each panel, the *y* axis represents the distance along the 20-m isobath starting from the North West Cape as indicated by the color scale on panel (a). A logarithmic color scale is used for panels (e)–(h). The alongshore axis is positive in the northeastward direction, and the cross-shore axis is positive seaward.

Figures S9g and S9h). However, the role of sediment advection was not negligible everywhere, particularly in very nearshore areas, in areas deeper than 50 to 100 m, and during the decreasing phase of the turbidity events (i.e., when deposition overcame erosion).

These four TC events accounted for a large fraction of the total shelf suspended sediment fluxes over this 2-year period, with Iggy and Narelle making the largest contribution southwest of Barrow Island, while Lua and Rusty had a major impact further toward the northeast (Figure 10). Overall, the sediment fluxes induced by these TCs tended to be consistently southwestward, with only some northeastward fluxes occurring toward the shelf edge during Iggy and Narelle (Figure 10a), due to the delay in suspended sediments reaching the outer shelf and the current reversals that occurred after the passage of the TCs.

4.1.2. Model Results: 14-Year Period

To assess the longer-term role of TCs to the shelf sediment dynamics, we extended the simulation to a 14-year period when calibrated remote sensing data were available. For this analysis, we focused on the

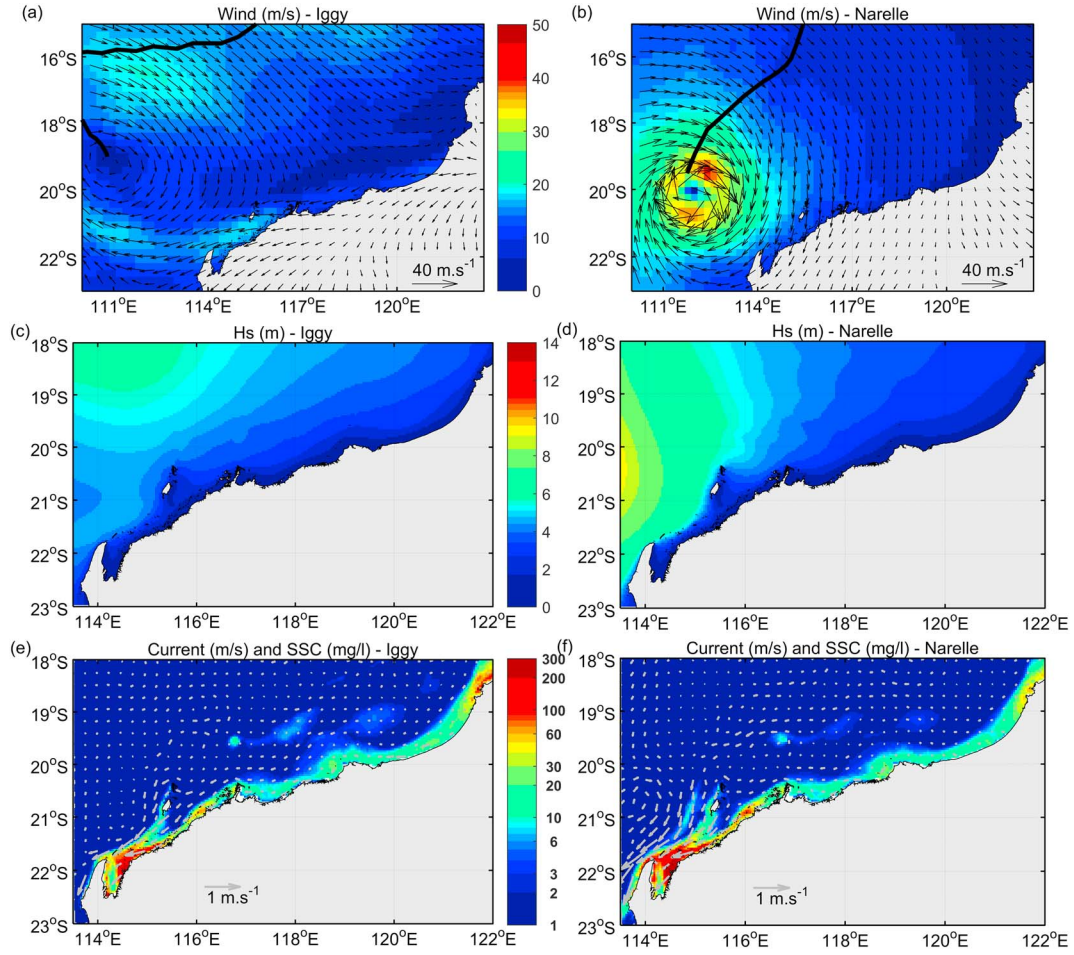

Figure 7. Wind (m/s) and significant wave height (m) during tropical cyclones (a and c) Iggy on the 27 January 2012 and (b and d) Narelle on the 12 January 2013. The cyclones tracks are indicated by the black lines. Daily averaged bottom SSC (color shading in logarithmic scale) and daily averaged depth-averaged current velocity (arrows) during (e) Iggy and (f) Narelle. SSC = suspended sediment concentration.

broad drivers of sediment dynamics over the entire NWS and thus also present average model results output along the 20-m isobath shown in Figure 6a. Similarly to what was simulated during the 2-year period, the main drivers of sediment dynamics over this 14-year period were the number of TCs that occurred (Figure 11). The main turbidity peaks were all related to wave events that occurred during TC events (Figures 11a, 11b, 11c, and 11e). Furthermore, during each of the TCs when SSC was elevated there were concomitant subtidal southwestward alongshore currents (Figure 11d), driving a dominant trend of southwestward suspended sediment fluxes over the entire shelf (Figure 11f). The southwestward alongshore currents occurred during increased alongshore wind events; indeed, over most of the shelf the alongshore currents were strongly correlated with alongshore wind (supporting information Figure S10). Along the 20-m isobath it therefore appeared that most of the alongshore sediment transport occurred during a smaller number of major TC events (Figure 11f). There was also a smaller cross-shore component to the suspended sediment flux, which was mostly related to TC events. This cross-shore flux resulted in an overall sediment export seaward of the 20-m isobath.

In particular, the TCs that generated the largest wave heights all coincided with the largest SSCs that occurred along the 20-m isobath (Figure 12a). All of those cyclones also induced significant southwestward alongshore currents. At the shelf scale there did not appear to be any preferential track for those TCs that had the greatest impact on sediment transport, with both shore-normal and shore-parallel propagating TCs having the capacity to generate substantial sediment erosion and transport (Figure 12b). However, in the southern

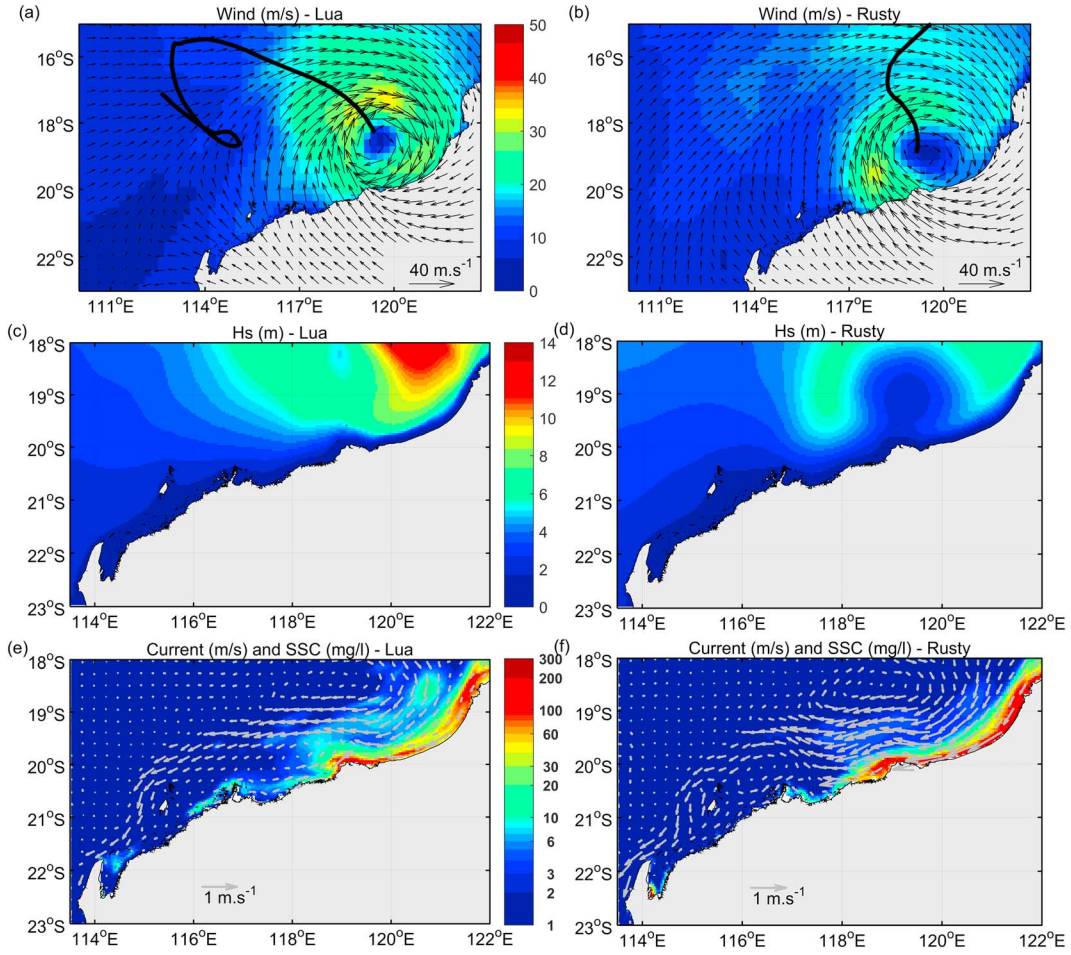

Figure 8. Wind (m/s) and significant wave height (m) during tropical cyclones (a and c) Lua on the 17 March 2012 and (b and d) Rusty on the 26 February 2013. The cyclones tracks are indicated by the black lines. Daily averaged bottom SSC (color shading in logarithmic scale) and daily averaged depth-averaged current velocity (arrows) during (e) Rusty and (f) Rusty. SSC = suspended sediment concentration.

section of the shelf (south of Barrow Island), most of the sediment transport happened during a few TCs (Nicholas, Bianca, Dianne, Carlos, Iggy, Narelle, and Quang) and all of them except for TC Quang had shore-parallel propagation tracks (Figure 12b).

Overall, we identified 19 cyclones (out of a total of 43) over the 14-year period (Fay, Daryl, Emma, Hubert, Glenda, George, Jacob, Nicholas, Laurence, Vince, Bianca, Dianne, Carlos, Iggy, Lua, Narelle, Rusty, Christine, and Quang) that played a major role on the sediment dynamics of the NWS (Figures 11e and 12a). During those 19 cyclones the suspended sediment fluxes over the shelf were primarily in the alongshore direction toward the southwest (Figure 13a). Those TC events, representing only 4.8% of the time of the 14-year time series, contributed to a large proportion of the total suspended load over most of the shelf, dominating (i.e., making a >50% contribution) over 80% of the shelf in depths shallower than the 100-m depth. Around Barrow Island and in the nearshore regions of the shelf from Barrow Island eastward, the contribution of TCs to the suspended load drastically decreased (Figure 13a). Indeed, TCs only dominated (>50% contribution) the suspended load over 45% of the shelf areas shallower than 20 m. There also appeared to be strong interannual variability in the sediment dynamics in response to the TCs, with 9 of the 19 energetic TCs occurring within just a 3-year period (January 2011 and December 2013) and inducing a large fraction of the total alongshore sediment fluxes (more than 60% of the total TC-induced flux along the 20-m isobath over the 14-year period; Figure 11e and Figure 11f). Although there was no obvious increase of the total number of cyclones during this period, the number of cyclones that had a significant impact on the sediment

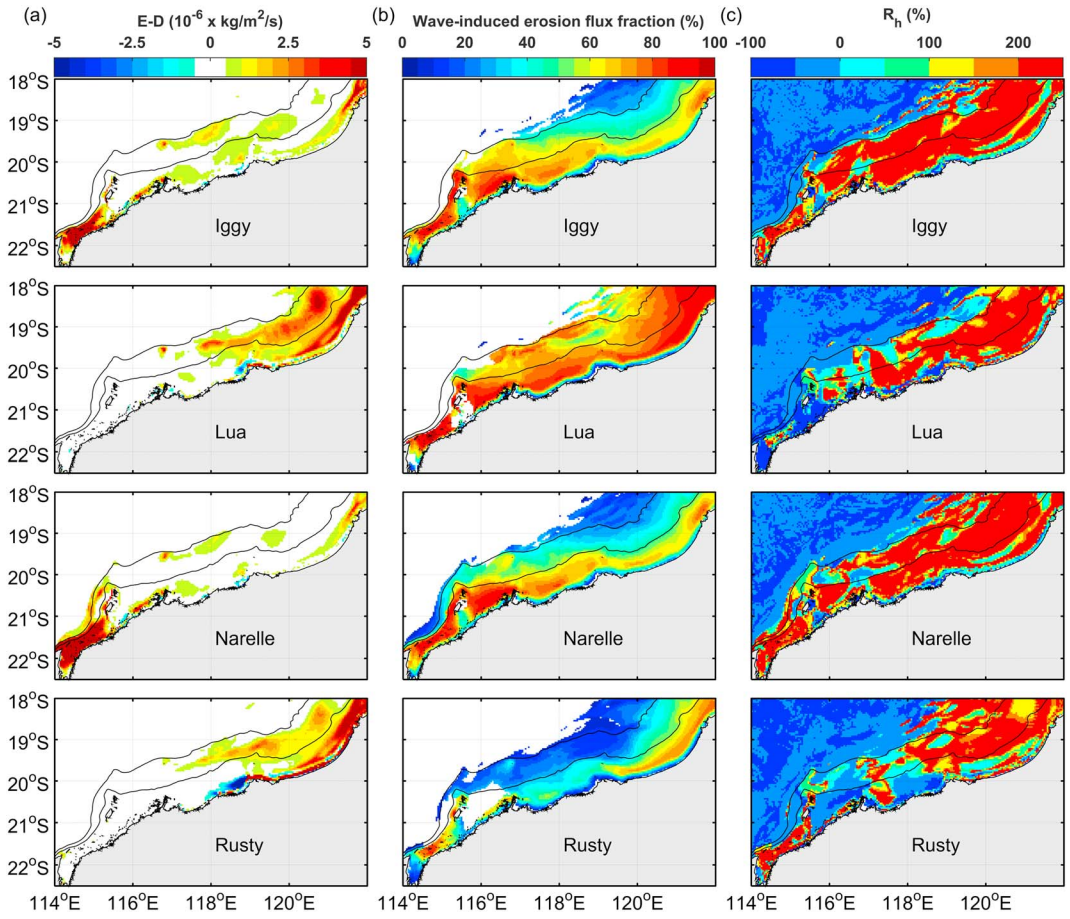

Figure 9. Fine sediment budget averaged over 2 days during Iggy (26–27 January 2012), Lua (16–17 March 2012), Narelle (11–12 January 2013), and Rusty (25–26 February 2013). (a) Net sediment flux at the seabed (erosion minus deposition). (b) Fraction of the total erosion flux induced by the wave-induced bottom shear stress. (c) *Vertical flux contribution* R_h (net sediment flux at the seabed divided by the absolute value of the sum of the horizontal advective and diffusive component of the depth-integrated suspended sediment concentration rate of change). Negative values denote areas where deposition dominate erosion and vice versa. The 50- and 100-m isobaths are indicated for reference on all maps.

dynamics increased. It appeared that both cyclone-induced wind and waves were stronger over the shelf and further offshore during this period (Figures 11b, 11c, and supporting information Figure S11a). Furthermore, the number of days per year with intense winds (>20 m/s) over the model domain was the highest during those three consecutive cyclone seasons and more than doubled compared to the mean value (~4 days per year; supporting information Figure S11b).

In terms of sediment export off the shelf, 12.5 Mt of fine suspended sediment were transported out of the 100-m isobath (over the ~850-km-long section, corresponding to sections 2 and 3 in Figure 14) during the 14 years, including 8.4 Mt during the 19 TCs. During those TC events, an additional 5.7 Mt of suspended sediment was predicted to exit the shelf through a relatively narrow (only ~20 km) cross-shelf section between the NW Cape and the 100-m isobath (section 1 in Figure 14), corresponding to 40% of the total TC-driven export (through section 1–3). Over that section at the southern end of the shelf, the sediment flux outside of TC events only accounted for 0.43 Mt, corresponding to ~7% of the total flux across that section. Overall, ~75% of the sediment export off the shelf was predicted to occur during the TC events that only occurred sporadically.

The patterns of sand bedload, while not the focus of this study, were slightly different to the suspended sediment patterns (Figure 13b). Although the strongest bedload fluxes still occurred during the TC events over most of the shelf, when integrating throughout the 14-year period, the relative contribution of the TCs was not as large (only dominating over 42% of the shelf in depths shallower than the 100-m depth) over the

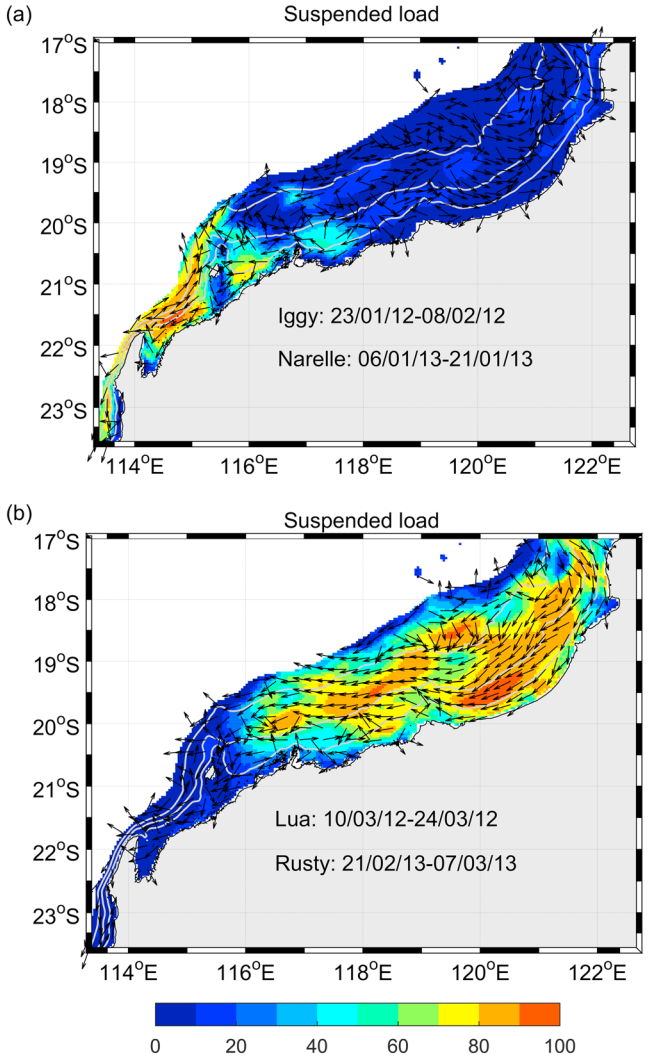

Figure 10. *TC contribution* R_{TC} (color shading in percent): Total depth-integrated suspended sediment flux for the period spanning May 2011 to March 2013 that occurred during (a) Iggy and Narelle and during (b) Rusty and Lua. The arrows indicate the direction of the cyclone-induced time-integrated suspended load. The 20-, 50-, and 100-m isobaths are indicated for reference. Only depth shallower than 200 m are considered.

shelf compared to the suspended load. There were even large areas, both nearshore and over some sections of the middle shelf, where the normal background (non-TC) forcing made up a large fraction of the total bedload transport. The residual (tidally averaged) sand bedload fluxes during TC events were generally in a southwestward to northwestward direction (Figure 13b).

5. Discussion

In this study we assessed the performance of a coupled wave-circulation-sediment transport model to investigate the processes that drive SSC variability and suspended sediment fluxes on Australia's NWS, integrating an extensive data set presented in a companion paper (Dufois et al., 2017) for validation. The model was applied to assess the relative role of waves and currents during the TC events and to evaluate the impact of episodic TCs compared to typical forcing (mostly tidally driven) at the shelf scale. We demonstrated that the cumulative impact of episodic TCs dominated the sediment dynamics over the entire shelf over the 14-year study period.

5.1. Sediment Dynamics During TC Events

Over the whole shelf, the model results suggested that both sediment resuspension and advection were episodically dominated by TC events. Our study confirmed the conclusions of Dufois et al. (2017) that focused on a small region of the NWS off Onslow over an ~2-year period when field observations were available, hence further emphasizing the role that TC-induced waves and currents play in driving the sediment dynamics over the entire NWS shelf at long timescales. Our results indicate that TCs on the NWS drive dominant and relatively consistent southwestward along-shelf suspended sediment fluxes. Cross-shelf suspended sediment fluxes, while much smaller, do play an important role in exporting sediments off the shelf. This supports the findings of Condie et al. (2009) who highlighted the role of a specific storm (TC Bobby) in exporting sediments off the shelf; our long-term study results confirm that this is a consistent feature of TCs on the NWS. Our results also suggested that a large fraction of the sediment export off the shelf occurred through a narrow (a ~20 km long) cross-shelf section near the North West Cape (section 1 in Figure 14).

During the peak of TC events, the local SSC rates of change were generally found to be driven by local wave-induced resuspension and hence not by either current-induced resuspension or advection. In other words, variability in SSC could largely be explained by local suspension of sediment by the energetic TC-generated waves despite strong currents also occurring on the shelf during the storms. However, within 10 to 20 km from the coast, current-induced resuspension and advection did often play a significant role during TC events, especially in the northern section of the shelf. The relative contribution of erosion and advection is, however, dependent on the sediment settling velocity, especially during the trailing edge of the turbidity events, with higher settling velocities reducing the residence time of the suspended sediments and therefore decreasing the relative contribution of advection, and vice versa. The best model performance was obtained using a value of 0.1 mm/s, corresponding to the settling velocity of small mud floc (Soulsby et al., 2013; Verney et al., 2009). However, using the data from the sediment traps moored at the seabed with the turbidity sensors used in our study, Sun and Branson (2018) estimated settling velocities ranging higher values of ~0.2–10 mm/s over the 2011–2013 period, consistent with larger mud flocs. Although sediment traps could probably exacerbate or reduce the downward sediment fluxes (Storlazzi et al., 2011) and hence strongly bias those estimations, we acknowledge that further in situ studies, including settling velocity and SSC vertical structure measurements, could be beneficial to better parametrize the model and strengthen our findings.

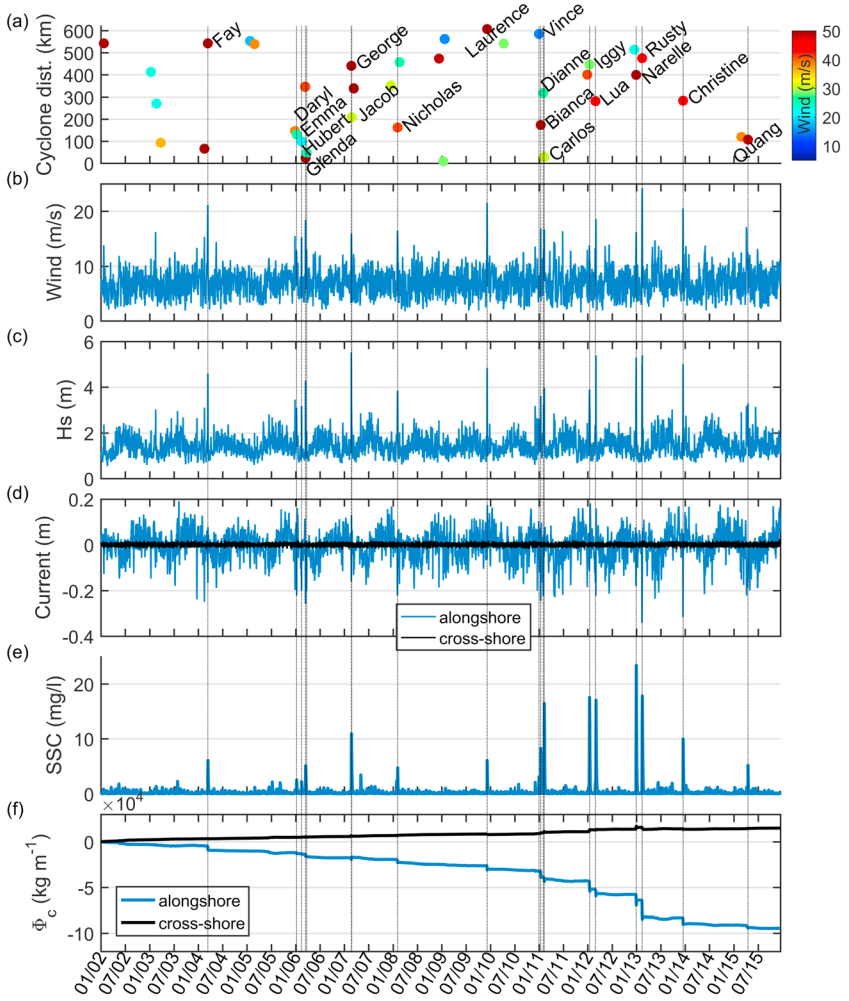

Figure 11. Daily averaged sediment dynamics simulated by the model along the 20-m isobath showed in Figure 6a for the period spanning January 2012 to December 2015. (a) Minimum distance from the cyclone centers to Onslow and maximum wind velocity during the cyclone lifespans. (b) Maximum wind strength and (c) significant wave height along the 20-m isobath. (d) Mean (along the 20-m isobath) depth-averaged alongshore and cross-shore current velocity, (e) bottom sediment concentration, and (f) cumulative alongshore and cross-shore depth-integrated sediment fluxes. The name of the cyclones that have a significant impact on the sediment dynamics is indicated on panel (a) and is highlighted by vertical dash lines striking through the whole figure. The alongshore axis is positive in the northeastward direction, and the cross-shore axis is positive seaward. SSC = suspended sediment concentration.

Various studies have shown a strong potential of TCs to redistribute the sediments along the coastline and produce morphological changes (Batker et al., 2010; Cuttler et al., 2018; Day et al., 2007). In this study we mainly focused on the water column and did not consider the longer-term impactions on morphological change (either on the shelf or at the coastline). However, the model highlighted the potential of TCs to both induce erosion and transport and therefore to induce potential morphological changes at the shelf scale, although this would need to be confirmed with in situ data and records of historical bathymetric/topographic changes.

Gravity-driven turbidity flows can potentially represent a secondary source of cross-shore sediment transport at the shelf scale (Falcini et al., 2012; Friedrichs & Wright, 2004). It should be noted that gravity-driven sediment transport was not included in the model (i.e., no feedback between sediment concentration and density in the hydrodynamic model) and that the impact of this process (dependent on the sediment inputs, the shelf slope, and the wave energy) would need to be evaluated over the NWS. Furthermore, the subtidal barotropic currents in the cross-shelf direction tended to be relatively weak, and due to the lower signal, the model performance tended to be reduced in the cross-shelf direction. Altogether, we therefore

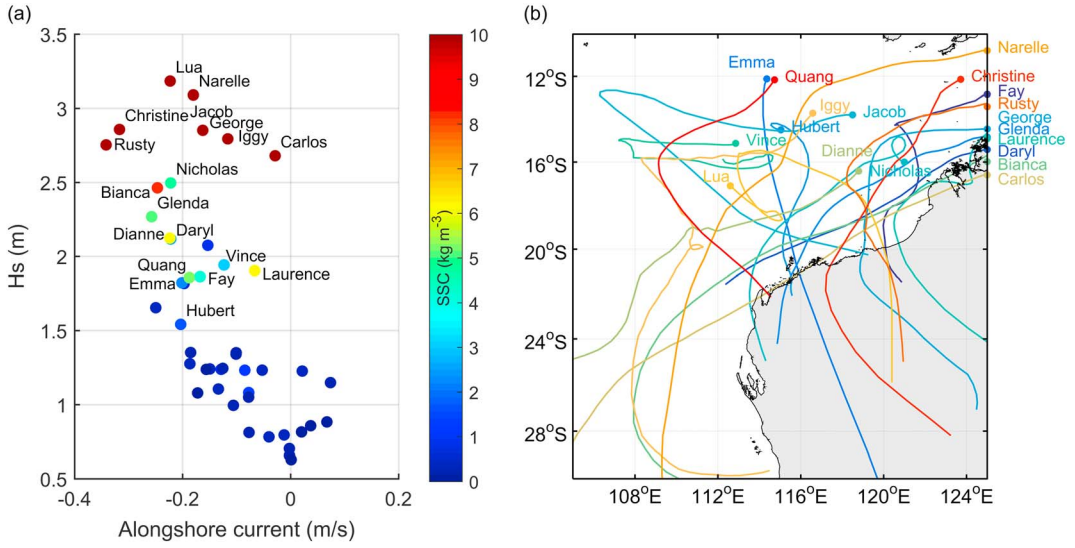

Figure 12. (a) Maximum significant wave height (m) versus minimum alongshore current velocity (i.e., maximum southeastward current), averaged over the 20-m isobath (showed in Figure 6a) during all TC events spanning June 2002 to December 2015. Color shading indicates the maximum bottom SSC (averaged over the 20-m isobath) occurring during each event. Cyclone names are given when $SSC > 1.5$ mg/L. (b) Track of the TCs with $SSC > 1.5$ mg/L (colored lines). The dots indicate the origin of the cyclone tracks. TC = tropical cyclone; SSC = suspended sediment concentration.

acknowledge that the estimation of the export fluxes in the cross-shelf direction contains more uncertainties than in the alongshore direction.

5.2. Long-Term Model Projection: Background Forcing Versus TC Events

To our knowledge, this is the first study applying a process-based numerical model (the ROMS-based COAWST model here) to simulate in detail the long-term (decadal) influence of TCs on sediment dynamics of a shelf. Process-based hydrodynamic-sediment transport models are usually deployed and validated over short time periods focusing on the responses to particular TC activity (Beudin et al., 2017; Miles et al., 2015; Palinkas et al., 2014; Warner et al., 2010; Xu et al., 2016). In this study we used an extensive 2-year-long in situ data set that captured two TCs with large impact and two TCs with lower impact in order to support our model deployment. The model performed reasonably well and gave us confidence in the longer-term model predictions.

Our modeling results indicated that even over long timescales, the TC-induced sediment fluxes dominated over most of the shelf (from the North West Cape in the south until at least Broome in the north), except close to the coast. In areas within ~10 to 20 km from the coast, especially over the northern part of the shelf, the typical background forcing (including the relatively strong tides) induced significant suspended load and bedload compared to TCs. As previously noted, those areas also correspond to regions where currents were a major driver of the sediment dynamics during TCs. However, those conclusions do not include any very nearshore areas (including beaches and tidal flats) where waves and surf zone processes would be expected to have a significant influence, due to the relatively coarse model resolution used in this study.

Conflicting studies have focused on identifying the hydrodynamic mechanisms that drive sediment transport on the NWS, with some proposing that the strong tides could overcome the impact of TCs on sediment resuspension over much larger section of the shelf, particularly as the tidal range increases toward the northeast (Harris et al., 2000; Porter-Smith et al., 2004). However, these studies have only considered sediment erosion potential (based on hydrodynamic predictions alone) but not sediment fluxes and did not use critical shear stress for bed motion but critical velocity using different formulations for waves and currents. In the present study we found that the critical shear stress is the parameter that had the major impact on the sediment dynamics overall pattern, including the relative contribution of extreme events versus background conditions. We adopted the formulation of Wilcock (1993) where the critical

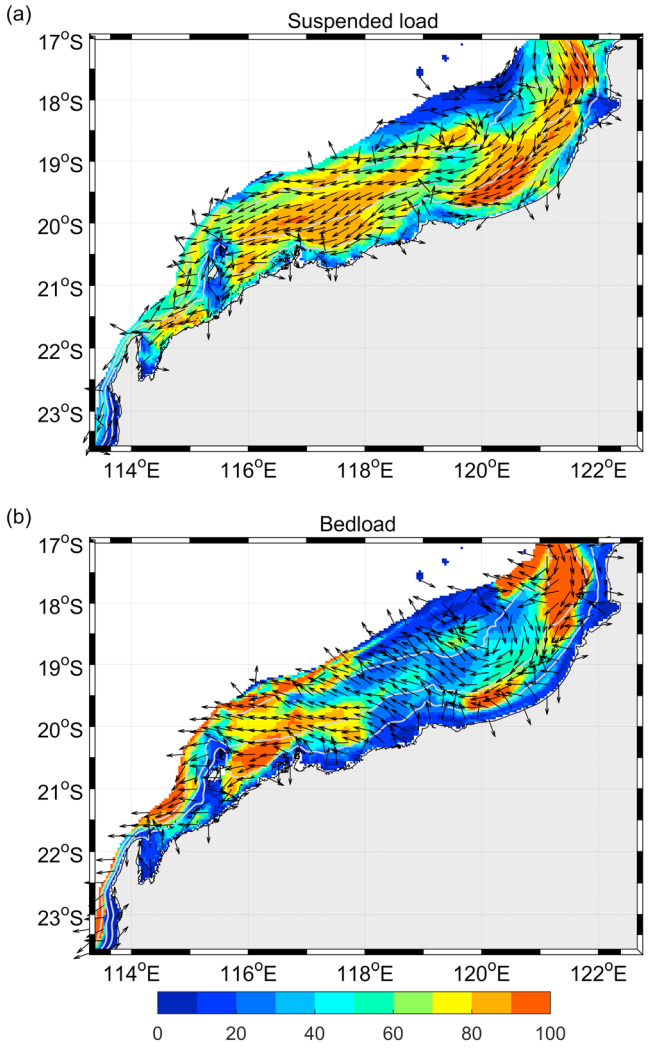

Figure 13. Contribution of 19 cyclones (Fay, Daryl, Emma, Hubert, Glenda, George, Jacob, Nicholas, Laurence, Vince, Bianca, Dianne, Carlos, Iggy, Lua, Narelle, Rusty, Christine, and Quang) to the 14-year (June 2002 to December 2015) sediment pathways. Only depth shallower than 200 m is considered. (a) Fraction R_{TC} (color shading in percent) of the total depth-averaged suspended sediment flux that occurred during cyclone events. The arrows indicate the direction of the cyclone-induced time-integrated suspended load. (b) Fraction R_{TC} (color shading in percent) of total bedload that occurred during cyclone events. The arrows indicate the direction of the cyclone-induced time-integrated bedload.

shear stress is similar for all sediment classes and based on the Shields value calculated for the mean sediment mixture diameter. This formulation gave the best model performance when comparing with the in situ data. At two locations off Onslow the modeled critical shear stress values (0.97 and 0.94 N/m^2) were close to the range of values (0.71 and 0.81 N/m^2) estimated in Dufois et al. (2017). No in situ suspended sediment data were available to validate the model in the northern region of the shelf (only remote sensing data were used). In the future, the monitoring of the sediment dynamics over the northern part of the shelf under TC conditions would be necessary to further reinforce our findings. In particular, the processes of segregation, hiding, and erosion of the fine sediment classes in a coarse sediment matrix are complex and further in situ studies (sediment dynamics and erodibility) should be carried out to confirm that the formulation that we choose is optimal at the scale of the whole shelf and lead to correct estimates of the sediment fluxes over the northern region of the shelf.

5.3. TC Variability

Although the model simulated an average (i.e., integrated over the TC) southwestward sediment flux, there was some intrastorm variability. Indeed, following the maximum turbidity generated by waves during each TC, a current reversal often occurred leading to some northeastward sediment fluxes, although weaker than the peak southwestward flux. During the peak of the TC event, quasi-geostrophic continental shelf waves triggered by TCs over the NWS could be responsible for the southwestward flow (Eliot & Pattiaratchi, 2010). In most cases we observed that the wind and subtidal currents were phase locked, suggesting that only *forced* continental shelf waves (i.e., mode 0) consisting of a locally generated surge traveling with the synoptic wind forcing under TCs (Eliot & Pattiaratchi, 2010; LeBlond & Mysak, 1978) were primarily acting.

Dufois et al. (2017) suggested that alongshore propagating TCs had the major sediment erosion and transport impact off Onslow. In this present paper we suggest that this could be more broadly the case for the shelf south of Barrow Island. Over the 14-year period, mostly alongshore propagating TC impacted the southern part of the shelf because TCs making landfalls tend to hit the coast further north, without inducing significant sediment resuspension and subtidal currents over the southern part. However, for the shelf section north of Barrow Island it appeared that the cyclone track had less importance than its strength and associated wind and wave field, with the track mostly determining the areas of most impact.

Interannual variability of TC activity over the NWS has been reported in the past, but no clear relationship with any common climate index has been found (Kevin & Lance, 2010). In our study we did observe strong interannual variability in terms of the sediment dynamics on the NWS due to the increased TC activity during the austral summers of 2011–2013. This period coincided with three consecutive Ningaloo Niño years, characterized by anomalously warm ocean conditions along the subtropical coast of Western Australia (Feng et al., 2015), which may have been responsible for the stronger cyclone intensity. There was, however, no clear direct relationship between the frequency and intensity of TC events and conventional El Niño–Southern Oscillation metrics. Indeed, usually only half of the Ningaloo Niño events occur during La Niña events (Feng et al., 2015). During the 2011–2013 period, the first 2 years coincided with La Niña years, while the 2012–2013 austral summer constituted a failed El Niño event resulting in a near neutral state (Corbett et al., 2017; Su et al., 2014).

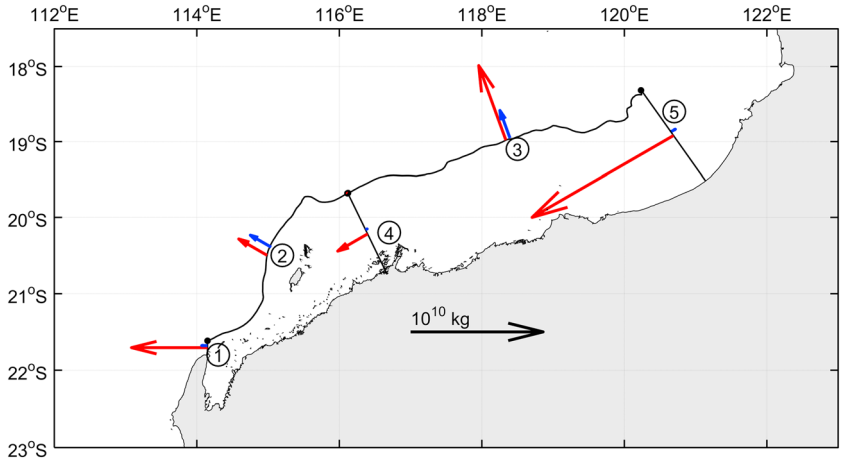

Figure 14. Suspended sediment fluxes across different sections simulated during the 14-year-long run. The red arrows correspond to the fluxes integrated during the 19 cyclones (Fay, Daryl, Emma, Hubert, Glenda, George, Jacob, Nicholas, Laurence, Vince, Bianca, Dianne, Carlos, Iggy, Lua, Narelle, Rusty, Christine, and Quang). The blue arrows correspond to the remainder of the sediment fluxes (i.e., the sum of the red and blue arrows correspond to the total sediment fluxes). The alongshore section follows the 100-m isobath. The black dots show the different numbered section boundaries.

6. Conclusions

Our study has revealed the overwhelming role that TCs play in driving sediment transport over most of the shelf over decadal timescales, despite individual events being relatively infrequent. The results also suggest that there can be strong interannual variability of the sediment dynamics on the NWS depending on TC activity in particular years that may be influenced by global climate drivers. While this has implications for the long-term sediment and habitat distribution over the shelf, this also has strong implications in terms of environmental impact assessments in the context of the ongoing marine developments over NWS. The 2-year-long data set obtained for the period May 2011 to March 2013 (Dufois et al., 2017) was originally motivated by the need to assess the baseline (natural) variability of the sediment dynamics on the NWS before a series of major dredging operations in the region. This data set includes a number of TCs that generated the largest sediment responses over the southern NWS. We therefore suggest that decadal to multidecadal modeling studies should be used to correctly assess the natural variability of the NWS. Indeed, due to the potentially large interannual variability in sediment dynamics, shorter-term modeling studies (e.g., those focusing on sediment transport by tides and regional currents) may significantly underestimate or overestimate the cumulative impact of extreme episodic events. In the future, assessing the role of more extreme TC activity under warming climate (Knutson et al., 2010; Webster et al., 2005) would be beneficial to better understand the long-term impact of TCs over the NWS.

Acknowledgments

This project was partially funded by the Western Australian Marine Science Institution (WAMSI) as part of the WAMSI Dredging Science Node, and made possible through investment from Woodside Energy, Chevron Australia, BHP Billiton as environmental offsets and by coinvestment from the WAMSI Joint Venture partners. Additional support was provided by the Australian Research Council Centre of Excellence for Coral Reef Studies. Data used in this study were partially provided by Chevron Australia as part of the Wheatstone project. The commercial investors and data providers had no role in the data analysis, data interpretation, and the decision to publish or in the preparation of the manuscript. The portion of the data related to the Wheatstone project can be requested for noncommercial use from WAMSI (info@wamsi.org.au) by establishing a data agreement. The processed and calibrated MODIS SSC data can be accessed through the National Computational Infrastructure data server available at http://remote-sensing.nci.org.au/. Additional mooring data were obtained from Australia's Integrated Marine Observing System (IMOS) available at https://portal.aodn.org.au/. Boundary conditions and forcing for the COAWST model were obtained from the Centre for Australian Weather and Climate Research (http://doi.org/10.4225/08/523168703DCC5) and from the Climate Forecast System (CFS) reanalysis (https://doi.org/10.5065/D6513W89). The model outputs used for the analyses performed in this paper have been archived on Zenodo (http://doi.org/10.5281/zenodo.1161904).

References

Ariathurai, R., & Arulanandan, K. (1978). Erosion rates of cohesive soils. *Journal of the Hydraulics Division*, *104*(2), 279–283.

Batker, D., Torre, I. D., Costanza, R., Swedeen, P., Day, J. W., Boumans, R., & Bagstad, K. (2010). Gaining ground: Wetlands, hurricanes, and the economy: The value of restoring the Mississippi River Delta*Rep*, 98 pp, Tacoma, Washington.

Battjes, J. A., & Janssen, J. (1978). Energy loss and set-up due to breaking of random waves, Proceedings of the Proceedings of 16th International Conference on Coastal Engineering, Hamburg, Germany.

Beudin, A., Ganju, N. K., Defne, Z., & Aretxabaleta, A. L. (2017). Physical response of a back-barrier estuary to a post-tropical cyclone. *Journal of Geophysical Research: Oceans*, *122*, 5888–5904. https://doi.org/10.1002/2016JC012344

Booij, N., Ris, R. C., & Holthuijsen, L. H. (1999). A third-generation wave model for coastal regions: 1. Model description and validation. *Journal of Geophysical Research*, *104*(C4), 7649–7666. https://doi.org/10.1029/98JC02622

Buffington, J. M., & Montgomery, D. R. (1997). A systematic analysis of eight decades of incipient motion studies, with special reference to gravel-bedded rivers. *Water Resources Research*, *33*(8), 1993–2029. https://doi.org/10.1029/96WR03190

Bunt, J. A. C., Larcombe, P., & Jago, C. F. (1999). Quantifying the response of optical backscatter devices and transmissometers to variations in suspended particulate matter. *Continental Shelf Research*, *19*(9), 1199–1220. https://doi.org/10.1016/S0278-4343(99)00018-7

Chapman, D. C. (1985). Numerical treatment of cross-shelf open boundaries in a barotropic coastal ocean model. *Journal of Physical Oceanography*, *15*(8), 1060–1075. https://doi.org/10.1175/1520-0485(1985)015<1060:NTOCSO>2.0.CO;2

Chassignet, E. P., Hurlburt, H. E., Smedstad, O. M., Halliwell, G. R., Hogan, P. J., Wallcraft, A. J., et al. (2007). The HYCOM (hybrid coordinate ocean model) data assimilative system. *Journal of Marine Systems*, *65*(1-4), 60–83. https://doi.org/10.1016/j.jmarsys.2005.09.016

Chevron (2011). Final environmental impact statement/response to submissions on the environmental review and management programme for the proposed Wheatstone project, *Technical Rep*., 337 pp, Chevron Australia Pty Limited, Australia.
Chevron (2016). Wheatstone project dredging and dredge spoil placement environmental monitoring and management plan, *Technical Rep. WS0–0000-HES-RPT-CVX-000-00086-000, Revision 4* Chevron Australia Pty Limited, Australia.
Condie, S., Herzfeld, M., Margvelashvili, N., & Andrewartha, J. R. (2009). Modeling the physical and biogeochemical response of a marine shelf system to a tropical cyclone. *Geophysical Research Letters*, *36*, L22603. https://doi.org/10.1029/2009GL039563
Corbett, C. M., Subrahmanyam, B., & Giese, B. S. (2017). A comparison of sea surface salinity in the equatorial Pacific Ocean during the 1997–1998, 2012–2013, and 2014–2015 ENSO events. *Climate Dynamics*, *49*(9-10), 3513–3526. https://doi.org/10.1007/s00382-017-3527-y
Cuttler, M. V., Hansen, J. E., Lowe, R. J., & Drost, E. J. (2018). Response of a fringing reef coastline to the direct impact of a tropical cyclone. *Limnology and Oceanography*, *3*, 31–38. https://doi.org/10.1002/lol2.10067
Day, J. W., et al. (2007). Restoration of the Mississippi Delta: Lessons from Hurricanes Katrina and Rita. *Science*, *315*(5819), 1679–1684. https://doi.org/10.1126/science.1137030
Dorji, P., Fearns, P., & Broomhall, M. (2016). A semi-analytic model for estimating total suspended sediment concentration in turbid coastal waters of northern Western Australia using MODIS-Aqua 250 m data. *Remote Sensing*, *8*(7), 556. https://doi.org/10.3390/rs8070556
Drost, E. J. F., Lowe, R. J., Ivey, G. N., Jones, N. L., & Péquignet, C. A. (2017). The effects of tropical cyclone characteristics on the surface wave fields in Australia's North West region. *Continental Shelf Research*, *139*, 35–53. https://doi.org/10.1016/j.csr.2017.03.006
Dufois, F., Lowe, R. J., Branson, P., & Fearns, P. (2017). Tropical cyclone-driven sediment dynamics over the Australian North West Shelf. *Journal of Geophysical Research: Oceans*, *122*, 10,225–10,244. https://doi.org/10.1002/2017JC013518
Durrant, T., Greenslade, D., Hemer, M., & Trenham, C. (2014). A global wave hindcast focussed on the central and South Pacific, *Technical Report Rep. 070*, 45 pp, CAWCR, Melbourne, Australia.
Egbert, G. D., & Erofeeva, S. Y. (2002). Efficient inverse modeling of barotropic ocean tides. *Journal of Atmospheric and Oceanic Technology*, *19*(2), 183–204. https://doi.org/10.1175/1520-0426(2002)019<0183:EIMOBO>2.0.CO;2
Egiazaroff, I. V. (1965). Calculation of nonuniform sediment concentrations. *Journal of the Hydraulics Division*, *91*(4), 225–247.
Eliot, M., & Pattiaratchi, C. (2010). Remote forcing of water levels by tropical cyclones in southwest Australia. *Continental Shelf Research*, *30*(14), 1549–1561. https://doi.org/10.1016/j.csr.2010.06.002
Falcini, F., Fagherazzi, S., & Jerolmack, D. J. (2012). Wave-supported sediment gravity flows currents: Effects of fluid-induced pressure gradients and flow width spreading. *Continental Shelf Research*, *33*, 37–50. https://doi.org/10.1016/j.csr.2011.11.004
Feng, M., Hendon, H. H., Xie, S.-P., Marshall, A. G., Schiller, A., Kosaka, Y., et al. (2015). Decadal increase in Ningaloo Niño since the late 1990s. *Geophysical Research Letters*, *42*, 104–112. https://doi.org/10.1002/2014GL062509
Friedrichs, C. T., & Wright, L. D. (2004). Gravity-driven sediment transport on the continental shelf: Implications for equilibrium profiles near river mouths. *Coastal Engineering*, *51*(8-9), 795–811. https://doi.org/10.1016/j.coastaleng.2004.07.010
Harris, P. T., Smith, R., Anderson, O., Coleman, R., & Greenslade, D. (2000). *GEOMAT—Modelling of continental shelf sediment mobility in support of Australia's regional marine planning process* (Geoscience Australia Record 41) (58 pp.). Canberra, Australia: Australian Geological Survey Organisation.
Hearn, C. J., & Holloway, P. E. (1990). A three-dimensional barotropic model of the response of the Australian North West Shelf to tropical cyclones. *Journal of Physical Oceanography*, *20*(1), 60–80. https://doi.org/10.1175/1520-0485(1990)020<0060:ATDBMO>2.0.CO;2
Hemer, M. A., Zieger, S., Durrant, T., O'Grady, J., Hoeke, R. K., McInnes, K. L., & Rosebrock, U. (2016). A revised assessment of Australia's national wave energy resource. *Renewable Energy*, *114*(A), 85–107. https://doi.org/10.1016/j.renene.2016.08.039
Hodges, K., Cobb, A., & Vidale, P. L. (2017). How well are tropical cyclones represented in reanalysis datasets? *Journal of Climate*, *30*(14), 5243–5264. https://doi.org/10.1175/jcli-d-16-0557.1
Kevin, H. G., & Lance, M. L. (2010). Interannual variability of northwest Australian tropical cyclones. *Journal of Climate*, *23*(17), 4538–4555. https://doi.org/10.1175/2010jcli3362.1
Knutson, T. R., McBride, J. L., Chan, J., Emanuel, K., Holland, G., Landsea, C., et al. (2010). Tropical cyclones and climate change. *Nature Geoscience*, *3*(3), 157–163. https://doi.org/10.1038/ngeo779
Larcombe, P., & Carter, R. M. (2004). Cyclone pumping, sediment partitioning and the development of the Great Barrier Reef shelf system: A review. *Quaternary Science Reviews*, *23*(1-2), 107–135. https://doi.org/10.1016/j.quascirev.2003.10.003
Larcombe, P., & Morrison-Saunders, A. (2017). Managing marine environments and decision-making requires better application of the physical sedimentary sciences. *Australasian Journal of Environmental Management*, *24*(2), 200–221. https://doi.org/10.1080/14486563.2017.1309694
LeBlond, P. H., & Mysak, L. A. (1978). *Waves in the ocean*, *Elsevier Oceanography Series* (p. 602). New York: Elsevier.
Lindemer, C. A., Plant, N. G., Puleo, J. A., Thompson, D. M., & Wamsley, T. V. (2010). Numerical simulation of a low-lying barrier island's morphological response to Hurricane Katrina. *Coastal Engineering*, *57*(11-12), 985–995. https://doi.org/10.1016/j.coastaleng.2010.06.004
Liu, J. T., Wang, Y.-H., Yang, R. J., Hsu, R. T., Kao, S.-J., Lin, H.-L., & Kuo, F. H. C. C. (2012). Cyclone-induced hyperpycnal turbidity currents in a submarine canyon. *Journal of Geophysical Research*, *117*, C04033. https://doi.org/10.1029/2011JC007630
Longley, I. M., Buessenschuett, C., Clydsdale, L., Cubitt, C. J., Davis, R. C., Johnson, M. K., et al. (2002). The North West Shelf of Australia—A Woodside perspective, proceedings of the petroleum exploration Society of Australia Symposium, the sedimentary basins of Western Australia 3, M. Keep and S.J. Moss, eds, Perth, Australia.
Madsen, J. D., Chambers, P. A., James, W. F., Koch, E. W., & Westlake, D. F. (2001). The interaction between water movement, sediment dynamics and submersed macrophytes. *Hydrobiologia*, *444*(1/3), 71–84. https://doi.org/10.1023/a:1017520800568
Madsen, O. S. (1994). Spectral wave-current bottom boundary layer flows, in *Coastal Engineering* 1994. *Proceedings of the 24th International Conference on Coastal Engineering, Kobe, Japan* edited, pp. 384–398.
Madsen, O. S., Poon, Y.-K., & Graber, H. C. (1988). Spectral wave attenuation by bottom friction: Theory, Proceedings of the 21st International Conference on Coastal Engineering, Costa del Sol-Malaga, Spain.
Margvelashvili, N. Y., Andrewartha, J. R., Condie, S. A., Herzfeld, M. G., Parslow, J. S., Sakov, P. V., & Waring, J. R. (2006). Modelling suspended sediment transport on Australia's North West Shelf, *Technical Rep. 7*, 43 pp, CSIRO, Australia.
Miles, T., Seroka, G., Kohut, J., Schofield, O., & Glenn, S. (2015). Glider observations and modeling of sediment transport in Hurricane Sandy. *Journal of Geophysical Research: Oceans*, *120*, 1771–1791. https://doi.org/10.1002/2014JC010474
Palinkas, C. M., Halka, J. P., Li, M., Sanford, L. P., & Cheng, P. (2014). Sediment deposition from tropical storms in the upper Chesapeake Bay: Field observations and model simulations. *Continental Shelf Research*, *86*, 6–16. https://doi.org/10.1016/j.csr.2013.09.012
Porter-Smith, R., Harris, P. T., Andersen, O. B., Coleman, R., Greenslade, D., & Jenkins, C. J. (2004). Classification of the Australian continental shelf based on predicted sediment threshold exceedance from tidal currents and swell waves. *Marine Geology*, *211*(1–2), 1–20. https://doi.org/10.1016/j.margeo.2004.05.031.

Rayson, M. D., Ivey, G. N., Jones, N. L., Lowe, R. J., Wake, G. W., & McConochie, J. D. (2015). Near-inertial ocean response to tropical cyclone forcing on the Australian North-West Shelf. *Journal of Geophysical Research: Oceans*, *120*, 7722–7751. https://doi.org/10.1002/2015JC010868

Rügner, H., Schwientek, M., Beckingham, B., Kuch, B., & Grathwohl, P. (2013). Turbidity as a proxy for total suspended solids (TSS) and particle facilitated pollutant transport in catchments. *Environmental Earth Sciences*, *69*(2), 373–380. https://doi.org/10.1007/s12665-013-2307-1

Saha, S., Moorthi, S., Pan, H.-L., Wu, X., Wang, J., Nadiga, S., et al. (2010). The NCEP climate forecast system reanalysis. *Bulletin of the American Meteorological Society*, *91*(8), 1015–1058. https://doi.org/10.1175/2010BAMS3001.1

Saha, S., Moorthi, S., Wu, X., Wang, J., Nadiga, S., Tripp, P., et al. (2014). The NCEP climate forecast system version 2. *Journal of Climate*, *27*(6), 2185–2208. https://doi.org/10.1175/JCLI-D-12-00823.1

Shchepetkin, A. F., & McWilliams, J. C. (2005). The regional oceanic modeling system (ROMS): A split-explicit, free-surface, topography-following-coordinate oceanic model. *Ocean Modelling*, *9*(4), 347–404. https://doi.org/10.1016/j.ocemod.2004.08.002

Sherman, C., Schmidt, W., Appeldoorn, R., Hutchinson, Y., Ruiz, H., Nemeth, M., et al. (2016). Sediment dynamics and their potential influence on insular-slope mesophotic coral ecosystems. *Continental Shelf Research*, *129*, 1–9. https://doi.org/10.1016/j.csr.2016.09.012

Soulsby, R. L., & Damgaard, J. S. (2005). Bedload sediment transport in coastal waters. *Coastal Engineering*, *52*(8), 673–689. https://doi.org/10.1016/j.coastaleng.2005.04.003

Soulsby, R. L., Manning, A. J., Spearman, J., & Whitehouse, R. J. S. (2013). Settling velocity and mass settling flux of flocculated estuarine sediments. *Marine Geology*, *339*, 1–12. https://doi.org/10.1016/j.margeo.2013.04.006

Stone, G. W., Liu, B., Pepper, D. A., & Wang, P. (2004). The importance of extratropical and tropical cyclones on the short-term evolution of barrier islands along the northern Gulf of Mexico, USA. *Marine Geology*, *210*(1-4), 63–78. https://doi.org/10.1016/j.margeo.2004.05.021

Storlazzi, C. D., Field, M. E., & Bothner, M. H. (2011). The use (and misuse) of sediment traps in coral reef environments: Theory, observations, and suggested protocols. *Coral Reefs*, *30*(1), 23–38. https://doi.org/10.1007/s00338-010-0705-3

Su, J., Xiang, B., Wang, B., & Li, T. C. G. L. (2014). Abrupt termination of the 2012 Pacific warming and its implication on ENSO prediction. *Geophysical Research Letters*, *41*, 9058–9064. https://doi.org/10.1002/2014gl062380

Sun, C., & Branson, P. (2018). Numerical modelling of dredge plumes. Western Australian Marine Science Institution Dredging Science Node, Theme 3, Project 3.4., *Technical Rep*., Perth, Australia.

Tian, T., Merico, A., Su, J., Staneva, J., Wiltshire, K., & Wirtz, K. (2009). Importance of resuspended sediment dynamics for the phytoplankton spring bloom in a coastal marine ecosystem. *Journal of Sea Research*, *62*(4), 214–228. https://doi.org/10.1016/j.seares.2009.04.001

van der Westhuysen, A. J., Zijlema, M., & Battjes, J. A. (2007). Nonlinear saturation-based whitecapping dissipation in SWAN for deep and shallow water. *Coastal Engineering*, *54*(2), 151–170. https://doi.org/10.1016/j.coastaleng.2006.08.006

van Rijn, L. C. (1984). Sediment pick-up functions. *Journal of Hydraulic Engineering*, *110*(10), 1494–1502. https://doi.org/10.1061/(ASCE)0733-9429(1984)110:10(1494)

van Rijn, L. C. (2007). Unified view of sediment transport by currents and waves. III: Graded beds. *Journal of Hydraulic Engineering*, *133*(7), 761–775. https://doi.org/10.1061/(ASCE)0733-9429(2007)133:7(761)

Verney, R., Lafite, R., & Brun-Cottan, J.-C. (2009). Flocculation potential of estuarine particles: The importance of environmental factors and of the spatial and seasonal variability of suspended particulate matter. *Estuaries and Coasts*, *32*(4), 678–693. https://doi.org/10.1007/s12237-009-9160-1

Wang, P., Kirby, J. H., Haber, J. D., Horwitz, M. H., Knorr, P. O., & Krock, J. R. (2006). Morphological and sedimentological impacts of Hurricane Ivan and immediate poststorm beach recovery along the northwestern Florida barrier-island coasts. *Journal of Coastal Research*, *226*, 1382–1402. https://doi.org/10.2112/05-0440.1

Warner, J. C., Armstrong, B., He, R., & Zambon, J. B. (2010). Development of a Coupled Ocean–Atmosphere–Wave–Sediment Transport (COAWST) modeling system. *Ocean Modelling*, *35*(3), 230–244. https://doi.org/10.1016/j.ocemod.2010.07.010

Warner, J. C., Sherwood, C. R., Arango, H. G., & Signell, R. P. (2005). Performance of four turbulence closure models implemented using a generic length scale method. *Ocean Modelling*, *8*(1–2), 81–113. https://doi.org/10.1016/j.ocemod.2003.12.003.

Warner, J. C., Sherwood, C. R., Signell, R. P., Harris, C. K., & Arango, H. G. (2008). Development of a three-dimensional, regional, coupled wave, current, and sediment-transport model. *Computers & Geosciences*, *34*(10), 1284–1306. https://doi.org/10.1016/j.cageo.2008.02.012

Webster, P. J., Holland, G. J., Curry, J. A., & Chang, H. R. (2005). Changes in tropical cyclone number, duration, and intensity in a warming environment. *Science*, *309*(5742), 1844–1846. https://doi.org/10.1126/science.1116448

Wiberg, P. L., & Harris, C. K. (1994). Ripple geometry in wave-dominated environments. *Journal of Geophysical Research*, *99*(C1), 775–789. https://doi.org/10.1029/93JC02726

Wilcock, P. R. (1993). Critical shear stress of natural sediments. *Journal of Hydraulic Engineering*, *119*(4), 491–505. https://doi.org/10.1061/(ASCE)0733-9429(1993)119:4(491)

Willmott, C. J. (1982). Some comments on the evaluation of model performance. *Bulletin of the American Meteorological Society*, *63*(11), 1309–1313. https://doi.org/10.1175/1520-0477(1982)063<1309:SCOTEO>2.0.CO;2

Wolanski, E., Fabricius, K. E., Cooper, T. F., & Humphrey, C. (2008). Wet season fine sediment dynamics on the inner shelf of the Great Barrier Reef. *Estuarine, Coastal and Shelf Science*, *77*(4), 755–762. https://doi.org/10.1016/j.ecss.2007.10.014

Wu, W., Wang, S. S. Y., & Jia, Y. (2000). Nonuniform sediment transport in alluvial rivers. *Journal of Hydraulic Research*, *38*(6), 427–434. https://doi.org/10.1080/00221680009498296

Xu, K., Mickey, R. C., Chen, Q., Harris, C. K., Hetland, R. D., Hu, K., & Wang, J. (2016). Shelf sediment transport during hurricanes Katrina and Rita. *Computers & Geosciences*, *90*, 24–39. https://doi.org/10.1016/j.cageo.2015.10.009

Yan, L. (1987). An improved wind input source term for third generation ocean wave modelling *Rep. 0169–1651* (20 pp.) Royal Netherlands Meteorological Institute.

Erratum

In the originally published version of this article, there were a minor errors in the affiliations for co-authors Rayson and Branson and figure citations in sections 3.2 and 4.1.2. These have since been corrected and this version may be considered the authoritative version of record.